Middle to Late Pleistocene activity of the northern Matese fault system (southern Apennines, Italy)

Paolo Galli[1,2], Biagio Giaccio[2], Paolo Messina[2], Edoardo Peronace[2,3], Vincenzo Amato[4], Giuseppe Naso[1], Sebastian Nomade[5], Alison Pereira[5,6], Sabatino Piscitelli[7], Jessica Bellanova[7], Andrea Billi[2], Dominique Blamart[5], Antonio Galderisi[8], Alessandro Giocoli[9], Tony Stabile[7], Francoise Thil[5]

[1] Dipartimento della Protezione Civile Nazionale, Rome, Italy
[2] Consiglio Nazionale delle Ricerche, Istituto di Geologia Ambientale e Geoingegneria, Roma, Italy
[3] Università La Sapienza, Roma, Italy
[4] Università degli Studi del Molise, Isernia, Italy
[5] Laboratoire des Sciences du Climat et de L'Environnement, UMR8212, LSCE/IPSL, CEA-CNRS-UVSQ and SPU Université Paris-Saclay, Gif-Sur-Yvette, France
[6] Département de Préhistoire du Museum national d'Histoire naturelle, UMR 7194 du CNRS, 75013 Paris, France
[7] Consiglio Nazionale delle Ricerche, Istituto di Metodologie per l'Analisi, Potenza, Italy
[8] Università Federico II, Naples, Italy
[9] ENEA Casaccia, Roma, Italy

Corresponding author: Paolo Galli, Dipartimento Protezione Civile, Via Vitorchiano, 4 00189 Roma, Italy. (paolo.galli@protezionecivile.it).

Abstract. An integrated investigation, including geological, geomorphological, geophysical and structural survey, ^{14}C and tephrochronological ($^{40}Ar/^{39}Ar$ dating and major element and $^{87}Sr/^{86}Sr$ composition) analyses as well as paleoseismic trenching, along the N-Matese fault system (NMFS) is presented. The NW-SE trending, NE dipping, NMFS is ~28 km-long and is composed by five main segments – Mount Patalecchia fault (MPF), Colle di Mezzo fault (CMF), Roccamandolfi fault (RF), Bojano fault (BF), Colle della Defenza fault (CDF) – which we grouped in two main sub-systems; the Piedmont fault system (PFS, including MPF, CMF, RF and CDF, running along the Matese flanks) and the Bojano buried fault (BBF, matching the BF, bounding the present floodplain). The study allowed the characterization of the tectonic mobility of this structure as well as the associated Bojano basin sedimentary-tectonic evolution since the early Middle Pleistocene, providing also new clues concerning the fault historical activity and the associated Mw>6.5 earthquakes. We have found lines of evidence for >1 mm/yr slip rate along the presently BBF during the early-mid Middle Pleistocene, and similar rates for the main segments composing the PFS. The BBF significantly slowed down during the last 300 kyr, ceasing its activity before the Holocene. In turn, the segments of the PFS reactivated at the onset of Late Pleistocene, after a long period of quiescence (480-110 ka), with robust slip rates that would seem even accelerating in post LGM times. Paleoseismic data along the PFS suggest the occurrence of four Mw>6.6 earthquakes

in the past 3 ka, three of which match the little known 280 BC event, and the devastating 1456 and 1805 earthquakes.

Keywords: Active tectonics; paleoseismology; $^{40}Ar/^{39}Ar$ dating; Middle Pleistocene; Late Pleistocene; earthquakes; Apennines.

1. Introduction

There are plenty of villages and towns along the Apennine chain that have been repeatedly struck and destroyed by high magnitude earthquakes, the causative faults of which have never been recognized by geologists. These cases are an unpleasant rule in southern Italy, where the highly-erodible siliciclastic units do not allow the preservation of most geomorphological indications that, instead, let active faults be easily recognizable and traceable in the carbonate basin-and-range sectors of central Italy (Bosi, 1975; Galadini and Galli, 2000). By simply comparing the epicentral distribution of the highest magnitude events and known active faults (Fig. 1, right panel), it appears that between northern Calabria and the central Apennines only a handful of the largest historical earthquakes can be arguably associate to known, investigated active faults, as is the case of the Mount Marzano fault system (MMFS in Fig. 1, right panel), which actually affects an "island" of Meso-Cenozoic limestones surrounded by a “sea” of siliciclastic units (e.g., Mw~7.0 events of 989, 1694, 1980 recognized in paleoseismological trenches by Galli and Peronace, 2014).

In the southern Apennine, another carbonate massif likely prone to record the footprint of active tectonics are the Matese Mountains, a NW-SE trending, 50-km-long and 20-km-wide meso-cenozoic rocky ridge. The region surrounding the Matese massif is the mesoseismic area of several catastrophic earthquakes (Fig. 1), which caused the repeated destruction of the settlements founded there since pre-Roman times. Recently, one of these earthquakes (1349, September 9; Mw 6.6) has been paleoseismologically ascribed to the Aquae Iuliae fault (AIF in Fig. 1; Galli and Naso, 2009), a primary structure that bounds the southwestern edge of the massif, crossing the Volturno River and downthrowing its Middle-Late Pleistocene terraces below the Holocene plain (Galli et al., 2008a). To the north one of the mainshocks of the 1456 seismic sequence and the 1805 earthquake (both Mw>6.5) have been tentatively associated with the northern-Matese fault system (NMFS in Fig. 1; Galli et al, 2002; Porfido et al., 2002), a complex right-stepping normal fault system bounding the Bojano Quaternary basin.

However, to date, only sparse chronological and stratigraphical data are available for the Bojano basin Quaternary deposits (e.g. Di Bucci et al., 2005; Amato et al., 2014), making the assessment of the long term, Middle to Upper Pleistocene, activity of the MMFS, as well as of the general Quaternary

sedimentary-tectonic evolution of the basin, rather speculative and uncertain. In order to fill this gap, we performed an integrated geological and chronological study, including stratigraphical, structural, geomorphological and geophysical surveys, together with tephrochronological analyses ($^{40}Ar/^{39}Ar$ dating and major element and $^{87}Sr/^{86}Sr$ composition), ^{14}C dating, fault-scarp leveling and paleoseismic trenching, which provided new data to reliably frame both the Pleistocene tectonic-sedimentary evolution of the Bojano basin and the most recent activity of the NMFS, including the latest seismic sequence of January 2016 (Mw 4.4).

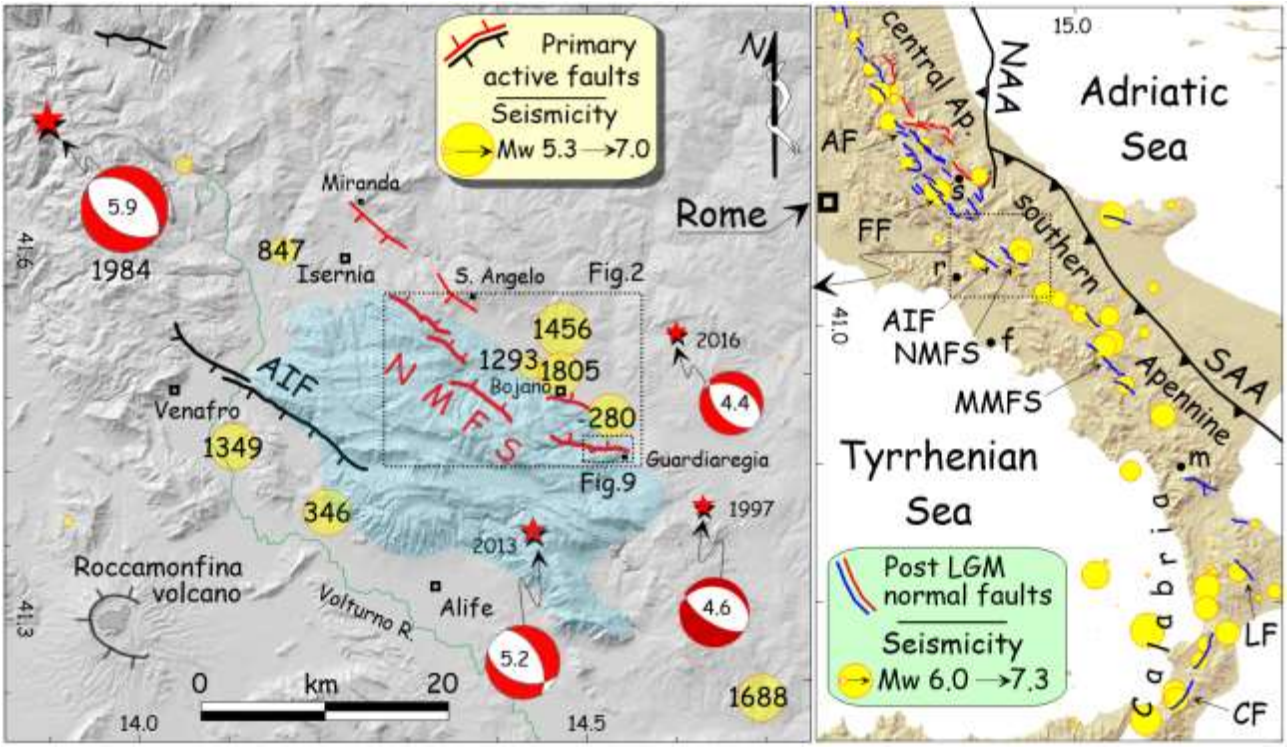

Fig. 1. Reference map of the investigated area. Left: epicenters of the strongest historical earthquakes (mod. from Galli and Naso, 2009) around the Matese massif (blue area) and primary active fault systems (AIF, Aquae Iuliae fault; NMFS, northern Matese fault system). Beach-balls are the focal mechanisms of the strongest instrumental events of the region (Pondrelli and Salimbeni, 2015), including the recent 2016 earthquake (QRCMT, 2016), all accounting for NE-SW extension. Note the location of Roccamonfina volcano, the main Middle Pleistocene source for the pyroclasts recognized in the investigated region. Right: primary post Last Glacial Maximum (LGM) faults along the Apennine chain, mostly investigated through paleoseismological studies (red, historically dormant faults. From Galli et al., 2008b), and highest magnitude earthquakes. NAA-SAA, northern and southern buried front of the Apennine thrusts. Fault systems cited in the main text: AF, upper Aterno; FF, Fucino; MMFS, Mount Marzano; LF, Lakes; CF, Cittanova. Labels r, f, m, s, Roccamonfina volcano, Phlegrean Fields (Campi Flegrei) volcano, Mercure basin, Sulmona basin, respectively.

2. Background

2.1. Hints on the seismotectonics of Apennines

The African-Eurasian plates collision (~7 mm/yr along a ~N-S direction over the past 11 Ma; Reilinger et al., 2006) and related Ionian slab subduction, drove the Neogene-Quaternary kinematic

evolution of the Mediterranean (Faccenna et al., 2004), and still drives the tectonics of the Italian peninsula mainly through the northward indenting of the Adria microplate (D'Agostino et al., 2008). This process causes active compression all along the Adria borders, with the growth of broad outer (Dinarides; southern Alps) and inner (northern Apennine Arc: NAA in Fig. 1, right panel) thrust systems.

With the exception of the southern Apenninic Arc (SAA; Fig. 1, right panel), where the compression front is no longer active since the Early-Middle Pleistocene (Cinque et al., 1993), these regional geodynamic processes result in a differentiation of the kinematics of the seismic sources, mainly composed by thrusting and transpressional faults all along the nortwestern to the eastern borders of Adria (i.e., from the Marche-Abruzzi offshore to the Po Plain, and to the Dinarides–Albanides, going clockwise). Conversely, along the Apennine chain, earthquakes are sourced by extensional faults resulting from a complex geodynamic mechanism (e.g. Pondrelli et al., 2006, and reference therein), which involves both the flexure-hinge retreat of the SW-subducting Ionian-Adriatic slab (i.e., contemporary to the Tyrrhenian basin opening), and the postorogenic gravitative collapse of the chain (Malinverno and Ryan, 1986; Royden et al., 1987; Patacca et al., 1990; 2008; Doglioni, 1991; Doglioni et al., 1994; D'Agostino et al., 2001).

Indeed, all the medium-strong earthquakes (6≤Mw≤7; see Working Group CPTI, 2011; CPTI11 hereinafter) from Tuscany to Calabria are sourced by NW-SE normal fault systems (NE-SW in southern Calabria) affecting the entire Apennine divide (Fig. 1, right panel). Faults generally bound intermountain basins (Lotti, 1915; Bosi, 1975; Galadini and Galli, 2000), accounting for a general NE-SW extension of the chain (Pierdominici and Heidbach, 2012), which has been currently estimated at ~2-4 mm/yr by GPS data analysis (D'Agostino et al., 2014).

In the investigated area, continuous GPS measures along a NE-SW transect (data from 1994 to 2007: Giuliani et al., 2009) have revealed net velocity steps north and south of the western Matese Massif which account for ~4-5 mm/yr NE-SW extension, partitioned between the northeastern (~1.8 mm/yr; 1.6±0.4 mm/yr in Ferranti et al., 2015) and southeastern (~2.7 mm/yr) flanks of the Matese Massif. The same extensional trend is also highlighted by the four focal mechanisms available in the area for Mw≥4.4 earthquakes (Fig. 1), all sharing a horizontal σ3 axis striking around 40° and 200° (see also Ferranti et al., 2015).

2.2. Seismicity of the investigated area

The region surrounding the Matese massif has been struck by destructive earthquakes (Io≥9 MCS, Mercalli-Cancani-Sieberg scale; Sieberg, 1930) on record mainly in the past millennium, i.e. the period for which written sources are mostly available (see epicenters in Fig. 1). The south-western

side was affected by the September 1349 (Mw 6.6, Io 10 MCS) and by the so-called 346 (Manetti, 1457) events. The former was undoubtedly sourced by the AIF (Galli and Naso, 2009), whereas the latter is likely composed by a seismic sequence started after 355 (Capini and Galli, 2003) and lasted several years during the 3rd quarter of the 4th century (Galadini and Galli, 2004). The southeastern side was hit by the June 1688 event (Mw 7.0, Io 11 MCS), the causative fault of which has never been identified. Finally, the northern sector has been the mesoseismic area of several high-magnitude events. In September 1293 (Castelli, 1993; Mw 5.8, Io 8.5 MCS), Bojano was hit by an earthquake that killed many inhabitants, destroying castles and villages facing the plain. Although severe damage was experienced also in other sparse localities in Campania and Molise, it is likely that the epicenter was close to the Bojano basin. Then, starting from December 4, 1456, the southern Apennines were struck by one of the most devastating sequence ever occurred in Italy (30,000-60,000 casualties), with at least three different epicentral areas, the southernmost matching the mentioned 1688 event (Mw 7.0), another falling in the Bojano basin (~Mw 7.0; Magri and Molin, 1984; Meletti et al., 1988) and other(s) in the Abruzzi region. In the Bojano basin, dozens of villages were razed to the ground (Is 10-11 MCS) and several thousands of people died. A twin event occurred again in the Bojano basin less than four centuries later, when, on July 26, 1805, a Mw 6.6 caused 5000 deaths, inducing Is 10 MCS in those villages already hit in 1456 (Esposito et al., 1987; Michetti et al., 2000). Last but not least, there is another strong earthquake on record for the Bojano area in the antiquity. It was discovered through archaeo-paleoseismic analyses in the Hercules' sanctuary of Campochiaro (easternmost segment of the NMFS in Fig. 1) by Galli et al. (2002) who dated the surface faulting and the destruction of the sanctuary area to the early 3rd century BC (i.e., ~280 BC).

None of the historical primary sources of the 1456 earthquake reports conclusive indications of ground breaks, neither here nor anywhere else in the whole mesoseismic areas. Conversely, many authors who described the 1805 effects provided reliable information concerning the opening of long chasms along the path of both the primary and antithetic splays of the NMFS (Fortini, 1805; Pepe, 1806; Poli, 1806; D'Onofrio, 1805; Duca della Torre, 1805), particularly along the eastern segments (e.g. in Porfido et al., 2002).

Finally, on January 2016, a seismic swarm affected the investigated area (INGV web site: http://iside.rm.ingv.it/). Two hundred 1<Ml<4.3 events occurred in the hanging wall of the NMFS (depths mainly between 6-13 km), with a Mw 4.4 mainshock sourced by a NW-SE normal fault (see focal mechanism in Fig. 1).

2.3. Geology of the investigated area

The Matese carbonate massif (highest peak: Mount Miletto, 2050 m a.s.l.) occupies an area of ~1000 km^2 within the southern Apennine fold-and-thrust belt (blue area in Fig. 1). It is mainly composed of inner shelf carbonates passing northward to shelf-slope carbonates (D'Argenio et al., 1973), with a Meso-Cenozoic paleogeography likely controlled by high-angle normal faults. These structures were successively tilted and cut by the basal detachment (Calabrò et al., 2003) during the Neogene overthrusting of the Apennine units (i.e. the Matese thrust sheet) over the Molisan siliciclastic units and the Apula Platform carbonates (Mostardini and Merlini, 1986; Patacca and Scandone, 2007; Ferranti et al., 2015). During the Quaternary, extension was mainly accommodated by NW-SE normal faults, which partly inverted favorably oriented structures inherited from the Neogene compressive phase (Ferranti, 1997; Caiazzo et al., 2006), as well as by Pliocene-Early Pleistocene, ~E-W high-angle transpressive faults, which mainly reactivated as dextral, transtensive splays. At present, the faults that bound the northern edge of the massif, facing the Bojano plain, are part of the Northern Matese fault system (NMFS, Galli and Galadini, 2003; Di Bucci et al., 2005; Ferrarini, 2009. Figs. 2 and 3).

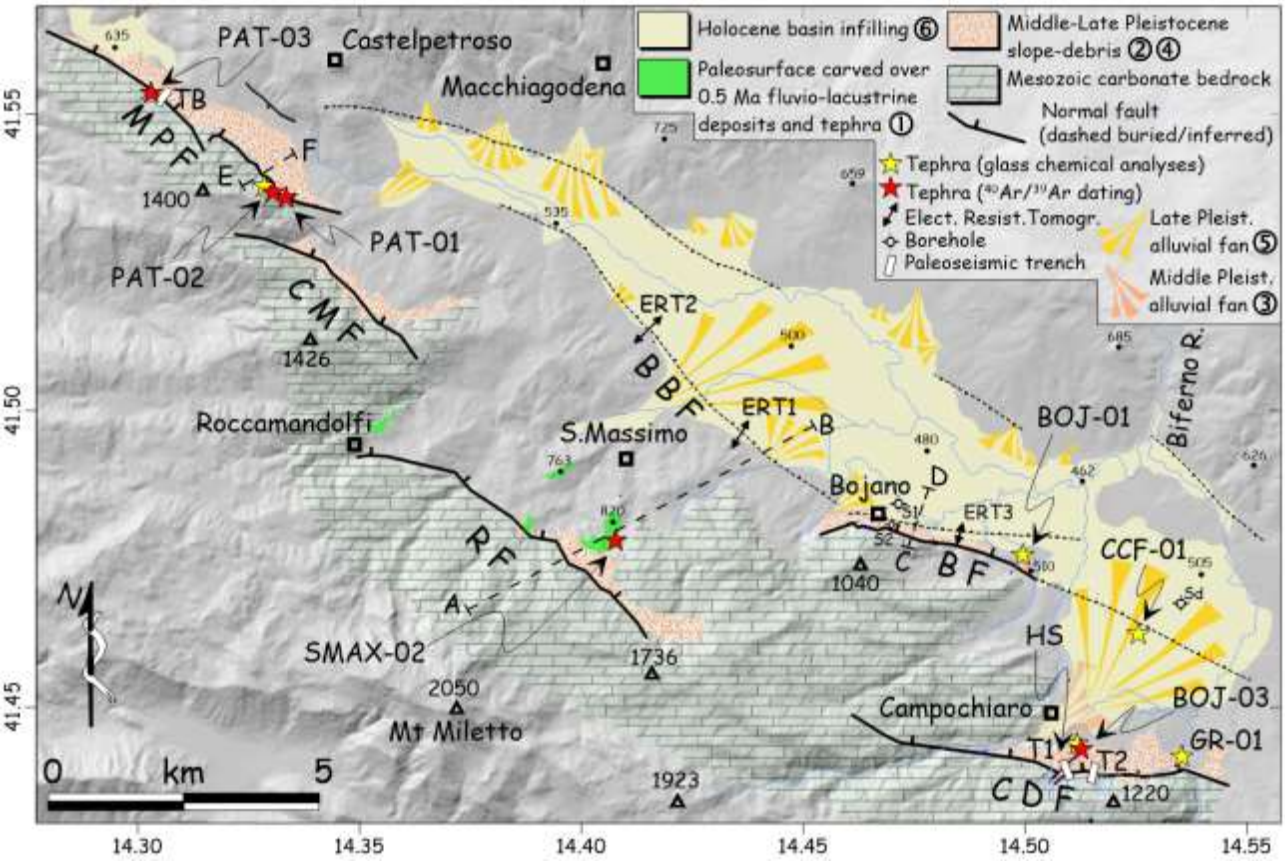

Fig. 2. Geological sketch, and investigation map of the northern Matese-Bojano Plain (see location in Fig. 1). MPF, Mount Patalecchia fault; CMF, Colle di Mezzo fault; RF, Roccamandolfi fault; BF, Bojano fault; CDF, Colle della Defenza fault; BBF, buried Bojano fault(s); T1, paleoseismic trench inside the Hercules' sanctuary (HS; Galli et al., 2002); T2, new trenching site (this paper); TB, trench in Blumetti et al. (2000); Sd, borehole reaching the bedrock 240 m below the ground surface; S1, boreholes in Amato et al. (2014); A-B, C-D, E-F, geological sections of Figs. 17, 18 and 20.

This structure is composed by different ~NW-SE normal fault segments with prominent bedrock-fault scarps (Figs. 3 and 4). Discontinuous antithetic splays run buried along the northern side of the Bojano plain (Blumetti et al., 2000; Porfido et al., 2002; Galli and Galadini, 2003; Di Bucci et al., 2005), and they outcrop only in the area from Castelpetroso toward Isernia (Figs. 1 and 2). The total length of the NE-dipping system is ~28 km, with five main segments ranging from 4 to 7 km. From NW to SE, these are the N305°-striking Mount Patalecchia fault (MPF in Fig. 2), made by two closely overlapping segments, the N315°-striking Colle di Mezzo fault (CMF), the N305°-striking Roccamandolfi fault (RF), the N290°-striking Bojano fault (BF), and the N280°-striking Colle della Defenza fault (CDF), which includes two overlapping segments (Fig. 2).

To the northeast, the Matese mountains slope toward the ~25-km-long, NW-SE elongated Bojano basin (~500 m a.s.l.), filled by Pleistocene fluvial-lacustrine deposits (Gemina, 1963). The alluvial plain of this basin is relatively narrow (<4 km), although the presence of fluvial-lacustrine deposits hanging along the southern slopes (~800 m a.s.l.; Figs. 2 and 4). San Massimo unit in Brancaccio et al., 1979) suggests that the basin was larger during the Middle Pleistocene, as suggested by $^{40}Ar/^{39}Ar$ dating made by Di Bucci et al. (2005) on tephra layered in this sediments (621±6 ka and 649±21 ka on samples San2 and San3, respectively). The basin is a half-graben, with a master fault system cropping out in the south and an antithetic system currently buried in the north (e.g. in Mazzoli et al., 2000). According to geophysical data (Bernabini et al., 2009; Romano, 2010) and available borehole logs (Amato et al., 2014 and reference therein), the thickness of the Quaternary deposits varies along the valley, reaching 250-300 m at the most. A recent 900-m-deep borehole in the southern sector of the basin (Sd in Fig. 2) drilled 80 m of Late Pleistocene alluvial fan gravels, overlaying 70 m of alternating fluvial-palustrine sands and clays, and alluvial fan gravels of Middle Pleistocene age, and 90 m of late Early Pleistocene lacustrine-palustrine deposits, before reaching at 240 m (280 m a.s.l.) the pre-Quaternary bedrock (Miocene Molise Flysch; Amato et al., 2016).

Fig. 3. View looking south of the Matese range from the northern flanks of the Bojano basin and main toponyms quoted in the text. The Northern Matese fault system roughly parallels the entire foothill from Mount Patalecchia (NW side) to Guardiaregia (SE side). The photos were shot from two distant sites (from elevation points 685 and 725 in Fig. 2, respectively) and have different scale.

The detailed stratigraphy and age of the fluvial-marshy and lacustrine-palustrine infilling have been investigated by Amato et al. (2014) on the basis of two boreholes drilled in the Bojano area (S1 and S2 in Fig. 1, 160 m and 70 m-deep, respectively). These authors distinguished three main stratigraphical units: *i*) a deeper one (~90 m thick), with alternating lacustrine-palustrine and fluvial-marsh depositional facies, ending upward slightly before 311±5 ka (age of tephra MOL10, correlated to the White Trachityc Tuff - WTT - from Roccamonfina volcano in Fig. 1), and containing below an older age of 426±6 ka (tephra MOL13); *ii*) an intermediate unit (~40 m thick), with alternating palustrine and fluvial-marshly facies, younger than 311±5 ka; *iii*) an upper unit made of alternating fluvial and marshly deposits (~30 m thick) containing a tephra (MOL3-4) chemically matching the Neapolitan Yellow Tuff eruption (NYT, Phlegrean Fields volcanic area; f in Fig. 1, right panel) of ~15 ka just 8 m below the ground surface (here at 482 m a.s.l.). Besides the San Massimo unit, other Quaternary deposits mantle the slopes of the Matese massif and they are both the remnant of the oldest fluvial-lacustrine infilling of the basin (Russo and Terribile, 1995; Guerrieri, 2000), and the typical climatogenic rudites sourced by the carbonate slopes during all the Pleistocene.

Fig. 4. Left: view looking SW of the Roccamandolfi fault scarp (Figs. 2 and 3) evidenced by the snow, and location of the raised San Massimo lacustrine deposits containing Middle Pleistocene tephra (star). Inset A is from Brancaccio et al. (1979), and shows the original outcrop with alternating fluvio-lacustrine deposits and pedogenized tephra levels. Star indicates location of our sample SMAX-02. Right: view looking SE of the rock fault scarp (i.e., fault mirrow or *nastro* in the Italian literature) of the northern segment of Northern Matese Fault System (Mount Patalecchia fault segment in Fig. 2). The arrow points to the southern tip of the Colle di Mezzo fault segment.

As far as the Quaternary activity of the NMFS is concerned, leaving aside the occurrence of bedrock fault scarps (the so called *nastri* in the Italian literature. See Fig. 4) - which may or may not imply the recent activity of the fault (e.g. Brancaccio et al., 1978; Cinque et al., 1991) - it is worth summarizing here some indications suggested by different authors in the past. Bosi et al. (1997) and Galli et al. (2002) highlight the presence of Pleistocene remnant land-surfaces carved in the hill slopes of Roccamandolfi, Cantalupo and Macchiagodena that outcrop at different elevation across the NMFS. Guerrieri et al. (1999) suggest that Middle Pleistocene to Late Glacial geomorphological features (e.g., slope scree and alluvial sediments) are systematically displaced along bedrock fault scarps. Blumetti et al. (2000) documented the offset of Holocene alluvial deposits inside a paleoseismic trench which they dug across the northern segment of the PFS (TB in Fig. 2), suggesting the occurrence of two strong earthquakes. Galli and Galadini (2003) provided the evidence for recent surface rupture along the CDF where – besides the faulting of a Last Glacial Maximum (LGM) alluvial fan (paleoseismic trench T1 in Fig. 2) – they also investigated the oblique offset of the *temenos*-wall and the buildings of the Hercules' Italic temple (HS in Fig. 2). Geomorphological indication of post LGM fault activity (i.e., topographic profiles across fault scarps) were also collected by Ferrarini (2009) along almost all the fault segments, although without any associated chronological constrain. All these previous studies described then the faulting of coarse carbonate, clast-supported

breccias along the fault-slopes of the NMFS (e.g., Bousquet et al., 1993), even if none of them provided radiometric ages for this ubiquitous formation.

3. Methods

3.1. Field investigations

We carried out field investigations over the entire mountainous area crossed by the NMFS (from 500 m a.s.l. to 1100 m a.s.l.). We integrated sedimentary facies and geological-structural analyses with geomorphological observations gathered in the field, from aerial stereopair photographs (1954 NATO photographs, 1:33.000 scale), from a digital terrain model (DTM) derived from the 1:5000-1:25000 topographic maps and, in places, from a 1-m-resolution LiDAR DTM (Bojano slope).

To obtain information on the kinematics of each single fault segment, we collected about 600 fault plane and *striae* orientations and analyzed them using the FaultKin5.2 and Stereonet7 software (Allmendinger et al., 2012). We used this software also to compute the local stress tensor through the inversion of the fault and striae attitude data. Specifically, we collected structural data in 125 stations located along the exposed fault surfaces running along the mountain slopes (29 stations along MPF; 9 along CMF; 29 along RF; 16 along BF; 42 along CDF; Fig. 2) that we here term Pediment Fault system (PFS), collecting almost 600 orientations of fault planes and related *striae* (i.e., the last and best preserved generation of *striae*). In computing the stress tensor, we assumed that slip on fault planes occurred in the direction of the resolved shear stress, and that the measured data reflect a uniform stress field, both spatially and temporally (Allmendinger et al., 2012).

3.2. High-precision topographic profiles

To identify the presence of compound fault scarps (*sensu* Wallace, 1977; 1984; Machette, 1986; 1987) and select a suitable site for paeoseismological trench investigations, we carried out microtopographic leveling across different fault segments. We realized the topographic profiles in areas where the fault scarp affects talus/alluvial deposits on both the footwall and the hanging wall. We followed the method proposed by Galli et al. (2014), who demonstrated that even in the Mediterranean area, the presence of enclosed forests may preserve the track of past strong earthquakes recorded as multiple breaks in the slope profile (e.g., inflection points). We manually carried out high-precision topographic profiles along the forested slopes of northern Matese. We measured fault scarps using an aluminum bubble triplometer, an optical hand-clinometer, and a fiberglass telescoping stadia rod, and applying the Roman cultellation method (i.e., knife arrangements). We spaced the elevation points along the profiles by about 1 m or less (i.e., 0.1-0.5 m across the fault zone and the edge of the retreated scarp), trying to avoid creep zones, holes, roots, and loose stones, and removing the thick depth of leaves.

3.3. Electrical Resistivity Tomography (ERT)

We investigated the subsurface architecture of the fault zone realizing three ERTs with a Syscal R2 (Iris Instruments) resistivity meter coupled with a multielectrode acquisition system (48 electrodes). We applied different array configurations (Wenner-Schlumberger and Dipole-Dipole), obtaining investigation depths ranging 25-80 m. We inverted the apparent resistivity data using the RES2DINV software (Loke, 2001) to obtain the 2D resistivity images of the subsurface. Further details on the methods concerning the Electrical Resistivity Tomography are provided in the Supplementary Materials.

3.4. Paleoseismic trenches

To identify past surface faulting events and large earthquake occurrences, two paleoseismic excavations were carried out both by hand digging - due to the impossibility for any excavator to reach some key sites in the steep (35°-40°) forested fault slopes - and by using a tracked-digger Hitachi ZX110, with a 1.2-m-wide bucket. After digging, we cleaned the exposed walls and equipped them with a 0.5-m-spaced cord grid, and then logged the sections exposed along the trench walls at a 1:20 scale.

3.5. Geochronology

To obtain reliable geochronological constraints for outlining the long term tectonic-sedimentary evolution of the basin and paleoseismological events, we performed a set of tephrochronological and radiocarbon analyses.

Tephrochronological investigations included major and minor element compositions, $^{40}Ar/^{39}Ar$ dating, and $^{87}Sr/^{86}Sr$ isotope analyses, on eight sub-primary to primary tephra layers found within the exposed lacustrine, alluvial fan, and slope deposits of the Bojano basin. Details on the realized analyses are summarized in Table 1, whereas the location of samples is shown in Figure 2.

Major and minor element compositions were determined using a wavelength-dispersive electron microprobe (WDS-EMPA) on glass shards and pumices from five out of eight collected tephra (Table 1). Analyses were carried out at the laboratories of the Istituto di Geologia Ambientale e Geoingegneria of the Italian National Research Council (IGAG-CNR) (Rome, Italy) using a Cameca SX50 electron microprobe (see methodological details in Giaccio et al., 2012; 2014).

$^{40}Ar/^{39}Ar$ dating was performed on pristine sanidine crystals extracted from five out of eight collected tephra (Table 1). Ar isotopes were analyzed using a VG5400 mass spectrometer at LSCE (Laboratory

of Science on climate and Environment, Gif-sur-Yvette, France) following procedures outlined in Nomade et al. (2010).

In situ Sr isotope compositions were determined on clino-pyroxene from three out of eight collected tephra (Table 1). Analyses were curried at LSCE (Laboratory of Science on climate and Environment, Gif-sur-Yvette, France) using a NWR193 ESI ablating system coupled with a Thermo Fisher MC-ICP Mass Spectrometer Neptuneplus. The instrument configuration used for the $^{87}Sr/^{86}Sr$ ratio determination is provided in Supplementary dataset DS3.

The radiocarbon dating for paleoseismological purposes was performed on four bulk samples collected in the trenches. ^{14}C analysis was performed at external scientific laboratories of the Beta Analytic company (Miami, USA) using the accelerator mass spectrometry technique in the. Standards and analytical protocols are both available online at http://www.radiocarbon.com/.

Table 1. Tephra sampled for tephrochronological analyses.

Samples	Environment	$^{40}Ar/^{39}Ar$	EMPA	$^{87}Sr/^{86}Sr$
SMAX-02	Lacustrine			
BOJ-01	Lacustrine			
BOJ-03	Alluvial fan			
GR-01	Alluvial fan			
CCF-01	Alluvial fan			
PAT-01	Slope			
PAT-02	Slope			
PAT-03	Slope			

4. Results

4.1. Stratigraphy of the Bojano Basin Quaternary deposits

4.1. 1. General framework

The results of the extensive geological-geomorphological surveys between the Bojano basin and the northern slopes of the Matese Massif allowed us to recognize several Quaternary units related to different depositional settings, variously deformed by the NMFS. According to the *facies* association, the general paleoenvironmental setting and the relative chronology, we identified, from bottom to top, five main units in the basin sedimentary infill: i.e., (*i*) *San Massimo terraced lacustrine deposits, (ii) Early slope-derived breccia,* (*iii*) *Terraced alluvial fan deposits,* (*iv*) *Late slope-derived deposits* and (*v*) *Late alluvial fan deposits*, along the slope and piedmont area, and (*vi*) *Lacustrine-palustrine-fluvial deposits* in the inner basin area

A synopsis of the stratigraphical results is provided in Figure 5. Starting from the oldest to the youngest deposits, and from the proximal to the distal settings, in the following sections we describe the lithological and geomorphological framework of these units.

353 *4.1.2. Slope and piedmont setting*

354 ***San Massimo terraced lacustrine deposits*** (1 in legend of Fig. 2). These are the oldest outcropping
355 sediments that we recognized in the Bojano Basin sedimentary infilling. They consist of alternating
356 clay and sandy levels capped by coarse gravel deposits. This unit is sporadically exposed as a deeply
357 eroded depositional terrace, the top elevation of which can be roughly estimated between 820 and
358 760 m a.s.l. (Fig. 2). In these deposits, we recognized and sampled a thick (~40 cm) tephra layer for
359 $^{40}Ar/^{39}Ar$ and $^{87}Sr/^{86}Sr$ (Table 1) analyses. This layer is exposed less than 7 m below the erosional
360 surface that caps the outcrop (SMAX-02, ~820 m a.s.l.; panel A in Fig. 4). The tephra SMAX-02 is
361 made of a coarse-grained base (Ø up to 1 cm) of pumice fall gradually turning into fine ash upward.
362 ***Early slope-derived breccia*** (2 in legend of Fig. 2). This unit consists of a coarse carbonate clast-
363 supported breccia discontinuously outcropping along the whole slope and piedmont area of the N-
364 Matese massif (Fig. 2). These deposits are commonly affected by the NMFS, with evident fault
365 damage zone, back tilting (40°-dipping), and other obvious fault-related features (Fig. 6).
366 Along the northern hillslope of Mount Patalecchia (785 m a.s.l.), in the hanging wall of one of the
367 MPF segments, this unit is unconformably overlain by a 2-m-thick, barely reworked pyroclastic fall
368 deposit made of cm-sized whitish-yellowish pumices (PAT-03; Figs. 2, 5 and 6). We sampled this
369 deposit for tephrochronological analyses ($^{40}Ar/^{39}Ar$; Tab. 1).
370 ***Terraced alluvial fan deposits*** (3 in legend of Fig. 2)**.** This unit comprises terraced conglomerates
371 exposed along the crest of the large Campochiaro alluvial fan (Fig. 2). These deposits subtend
372 remnants of a top depositional surface, which culminates at ca. 760 m a.s.l., i.e., 30 m above the
373 present *thalweg*. In these deposits, we found no suitable material for geochronological determinations
374 (e.g., tephra).
375

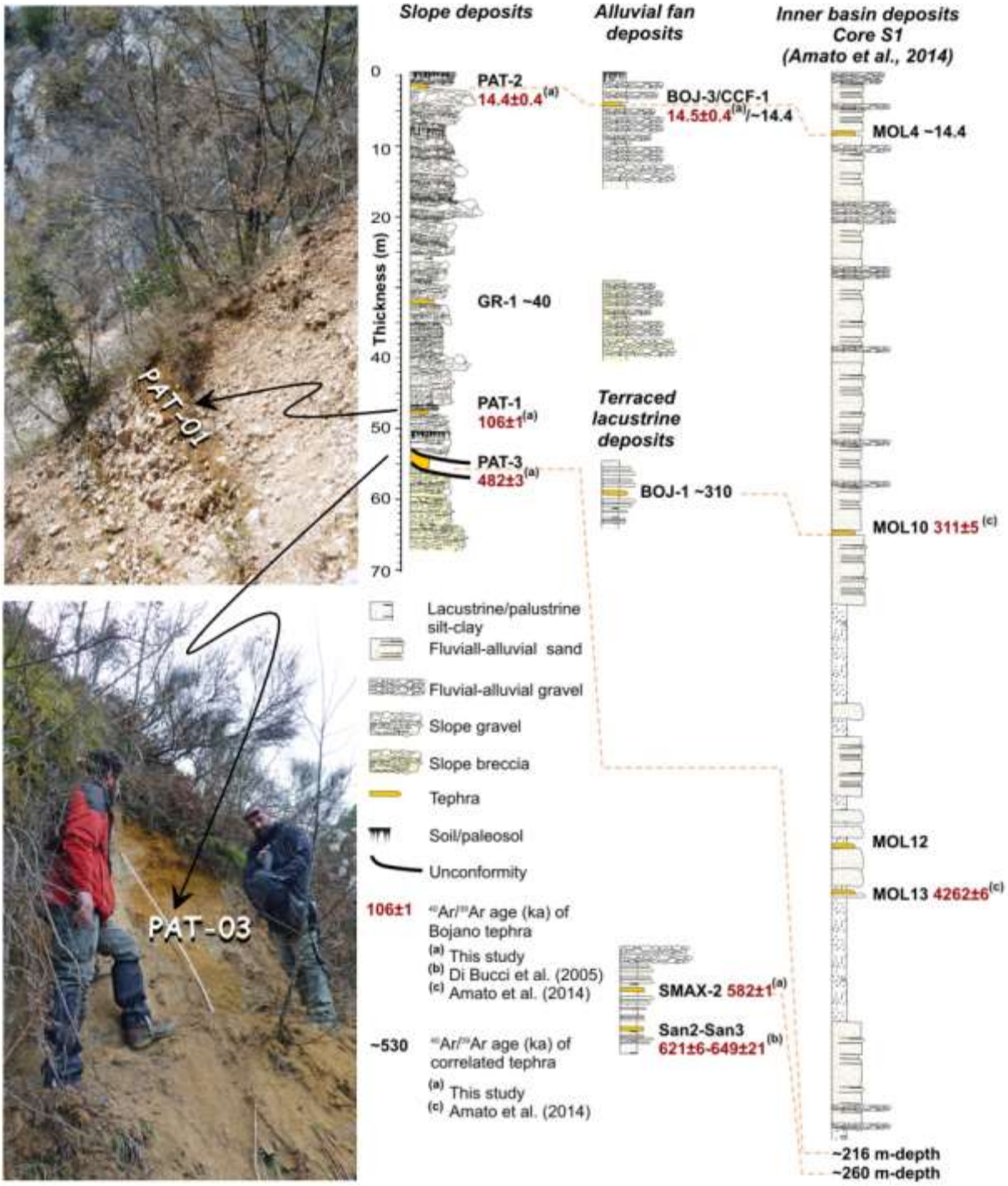

Fig. 5. Schematic stratigraphic sections for the main paleoenvironmental settings of the slope and piedmont areas (slope deposits, alluvial fan deposits and terraced lacustrine deposits) and of the inner basin (see Fig. 2 for site locations). The available chronological constrains from literature and from the present study are also shown.

Fig. 6. View looking NW of the fault between the carbonate bedrock (left) and the Middle Pleistocene (≥482 ka) slope breccias north to Mount Patalecchia (near PAT-03 site in Fig. 2). The active splay of the fault outcrops ~250 m downhill, where it offsets Holocene deposits.

Late slope-derived deposits (4 in legend of Fig. 2). This unit consists of stratified angular gravel with sandy levels and pedogenetic horizons that form the present talus of the N-Matese slopes (Fig. 2). Along the Mount Patalecchia slopes, the thickness of these deposits reaches ~50 m (Fig. 5). Usually, they unconformably lay on the Early slope-derived breccias, from which can be easily distinguished via lithological features and degree of the tectonics deformation (e.g. degree of cementation, grain-sizecoarser and counter-slope tilting).

We found a sub-primary tephra (PAT-01) occurring at the base of this unit along the left flank of a gully carved in the eastern Mount Patalecchia slope, at 900 m a.s.l., in the hanging wall of the MPF (Figs. 2, 5 and 6). We sampled this tephra for both $^{40}Ar/^{39}Ar$ dating and $^{87}Sr/^{86}Sr$ analysys (Table 1). The tephra PAT-01 is a 0.5-m-thick, orange, sandy sin-depositionally reworked and weathered volcanic layer rich in sanidine and clinopyroxene crystals, with up to 1-mm-sized pumices.

Less than 400 m away from the site where we sample PAT-01, the uppermost interval of the Late Pleistocene-Holocene slope-derived deposits is exposed (site PAT-02 in Fig. 2). At this locality, the angular gravels and colluvia, which were dragged and faulted along the fault plane, contain a 0.3-0.5 m-thick, brown-orange barely reworked volcanic layer mainly consistsing of highly vesicular coarse ash (2-3 mm-sized), which we sampled for both $^{40}Ar/^{39}Ar$ dating and glass WDS-EMPA analysys (Table 1). Moreover, we found and sampled another dm-thick yellowish tephra layer (GR-01) suitable for tephrochronological analyses (Table 1) in the basal-middle interval of this units cropping out in

the hanging wall of the CDF (Fig. 2). ***Late alluvial fan deposits*** (5 in legend of Fig. 2)**.** This unit comprises the wide system of active or sub-active alluvial fans, which spread in the present flood plain including the large Campochiaro and San Massimo fans and numerous secondary alluvial bodies (Fig. 2). The sediments of this system typically consist of alternating gravels, sandy levels, and pedogenetic horizons. The uppermost portion of the large Campochiaro fan, which extends in the whole southernmost sector of the Bojano basin (Fig. 2), contains a reworked ash layer (CCF-01), which we sampled for tephrochronological analyses (Table 1). We sampled also another primary tephra layer (BOJ-03; Table 1) occurring at the tip of the distal portion of an alluvial apron, which spreads in the hanging wall of the southernmost segment of the NMFS, namely the Colle della Defenza fault (CDF in Fig. 2). This fan telescopically develops from an older and larger alluvial fan fed by the Uma Valley (Fig. 7).

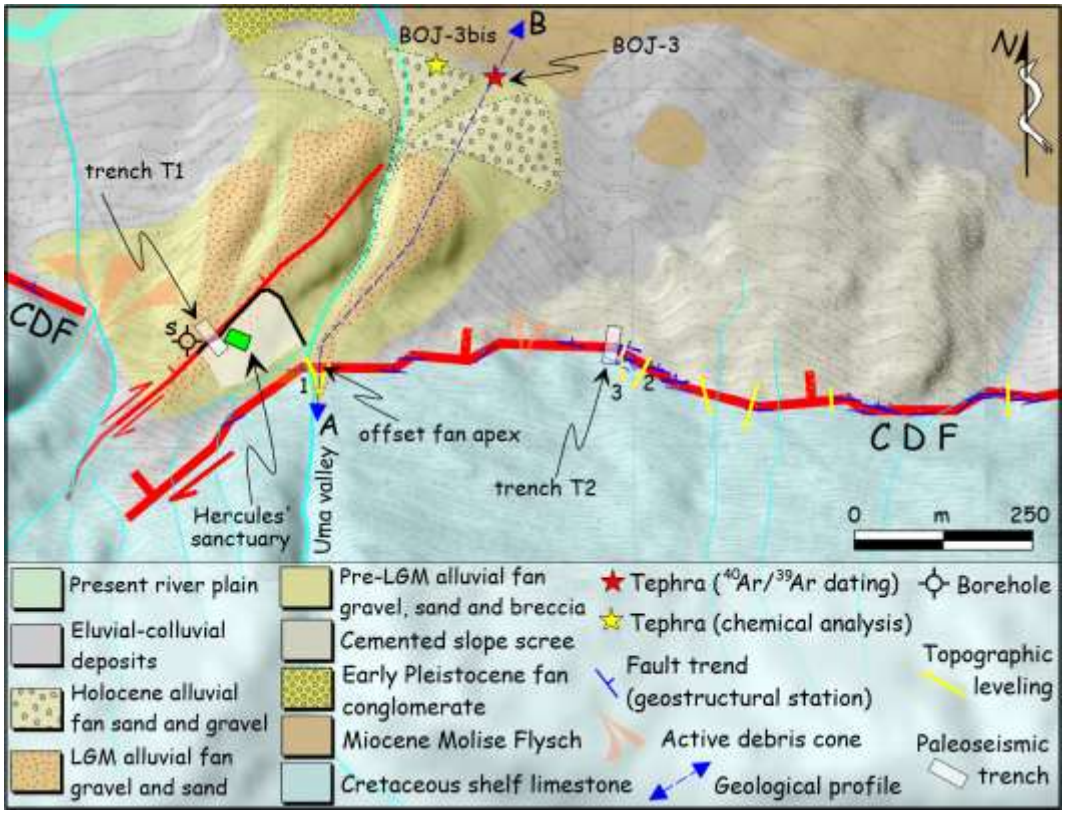

Fig. 7. Geological map of the west-tip of the Colle della Defenza fault (CDF Fig. 2). Note the NE-SW splay (thin red line) cutting through the accommodation zone between the two main CDF segments (bold red lines) that displaces also the Hercules' sanctuary area and the *temenos* wall (black line; s, borehole). A-B, geological section of Fig. 10. Stars indicates the tephra BOJ-03, chronologically and chemically correlated to the Neapolitan Yellow Tuff tephra (see section 5.1). Trench T1 is in Galli and Galadini (2003). Topographic profiles 1-2-3 are in Fig. 13. Background topography from 1:5000 maps.

4.1.3. Inner basin setting

Fluvial-palustrine-lacustrine deposits (6 in legend of Fig. 2). This sedimentary setting matches the subsurface succession of the present flood plain (see summary in section 2.3.). In the hanging wall of the Bojano fault (~500 m a.s.l.) we recognized lacustrine deposits made of grayish-brownish clay and silt containing a well-sorted level of white, vesicular, sub-aphyric, and up to 2-cm-sized pumices (BOJ-01), which we sampled for tephrochronological analyses (Tab. 1).

4.2. Tephrochronological results

Full analytical data of the $^{40}Ar/^{39}Ar$ dating, WDS-EMPA, and $^{87}Sr/^{86}Sr$ ratio determination are provided in Supplementary dataset DS1, DS2 and DS3, respectively. The results of $^{40}Ar/^{39}Ar$ analyses are displayed as age-probability density spectra in Figure 8 and summarized in Table 2. A synopsis of the WDS-EMPA results is provided as total alkali versus silica classification diagram (TAS, Le Maitre, 2002) in Figure 9. $^{87}Sr/^{86}Sr$ results are reported in Table 3. Results for individual layers are presented below. A brief lithological description of the tephra is reported in section 4.1.

SMAX-02 – Fifteen sanidine crystals extracted from SMAX-02 tephra in the San Massimo terraced lacustrine deposits yielded a homogeneous age-probability density spectra allowing us to calculate a weighted mean age of 582±1 ka (2σ; analytical uncertainty; Fig. 8). The $^{87}Sr/^{86}Sr$ ratio that we obtained by laser ablation analysis on thirteen clinopyroxenes is 0.7097±0.0008 (Table 3). We found no fresh glass shards suitable for WDS-EMPA analyses in SMAX-02.

PAT-01 – Ten sanidine crystals extracted from PAT-01 tephra provided a homogenous age-probability density spectra with weighted mean age of a 106±2 ka (2σ analytical uncertainty; Fig. 8). We found no fresh glass shards suitable for WDS-EMPA analyses in PAT-01.

PAT-02 – With the exception of an obvious xenocrystal, $^{40}Ar/^{39}Ar$ analysis on sanidine grains from PAT-02 displays a single population of crystals with a weighted mean age of 14.4±0.6 ka (2σ analytical uncertainty; Fig. 8). The composition of handpicked fresh glass shards from PAT-02 shows a relatively wide spectrum, which, in the TAS diagram, results in an elongated, linear trend parallel to the line separating the trachyte-phonolite and latite-tephriphonolite fields (Fig. 9). Twelve $^{87}Sr/^{86}Sr$ measurements of cpx from PAT-01 (Table 3) yielded a mean value of 0.70825±0.00059.

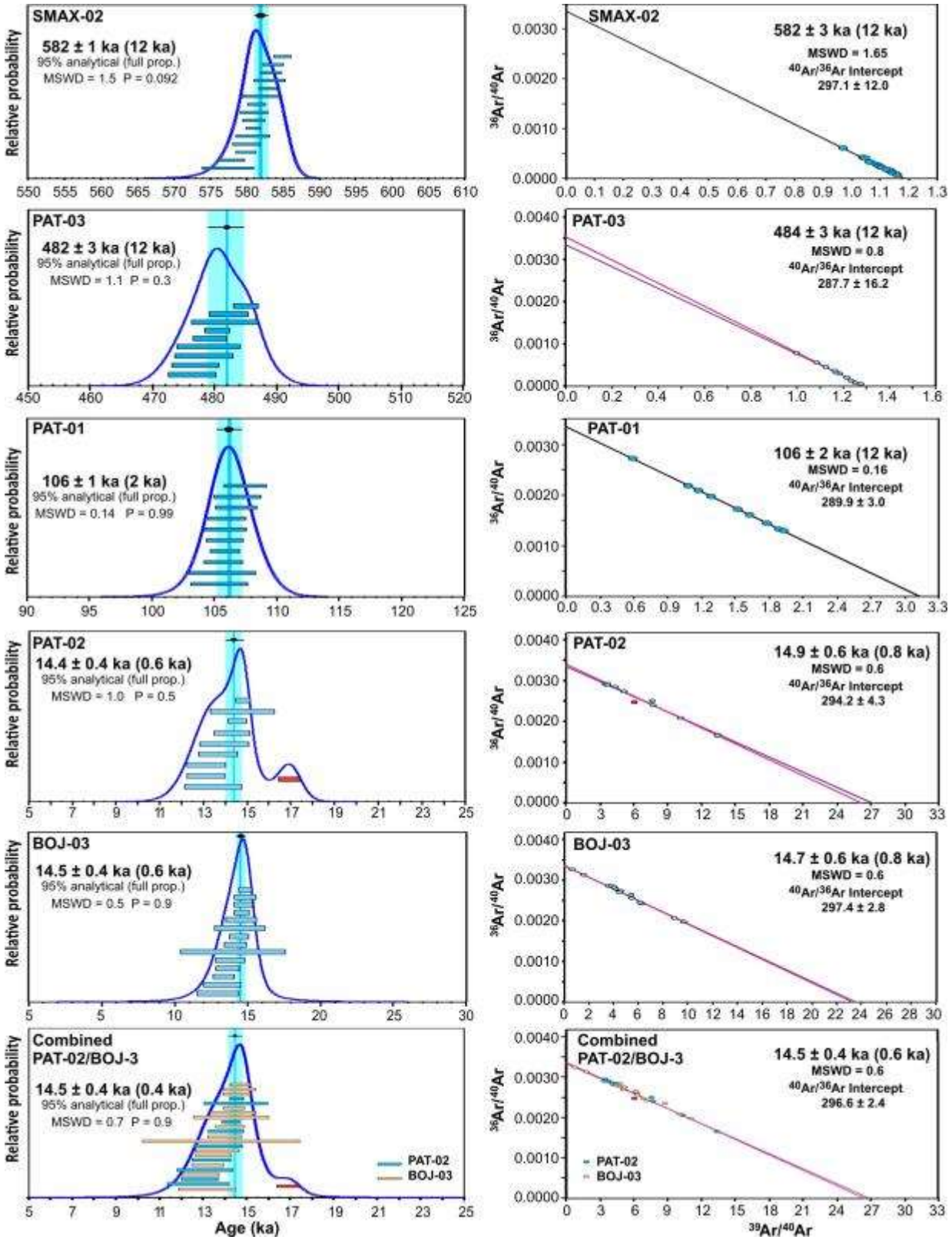

Fig. 8. Age probability density spectra diagrams (left) and inverse isochrons (right) for the investigated tephra from Matese basin. Blue-orange and red bars indicate the individual ages (width = 1σ error) included and discarded in weighted mean age, respectively.

PAT-03 – $^{40}Ar/^{39}Ar$ analysis of 9 sanidine crystals from PAT-03, occurring on top of the Early slope-derived breccia (Fig. 5), provided an age of 482±3 ka (2σ analytical uncertainty; Fig. 8). Juvenile clasts from PAT-03 are highly altered, making the tephra unsuitable for WDS-EMPA major element analysis.

GR-01 – The analyses of handpicked fresh glass shards extracted from the GR-01 tephra yielded a rather homogeneous trachytic composition with SiO_2 and alkali sum contents narrowing between 61.5 and 62.5 wt% and between 14 and 13 wt%, respectively (Fig. 9).

CCF-01 – Major element composition of the glass from this layer is bimodal, with two distinct trachyte (SiO_2 ~62-63 wt%) and latite (SiO_2 ~57-58 wt%) populations (Fig. 9).

BOJ-01 – The major element composition of the glassy pumices from BOJ-01 tephra depicts a high-silica trachyte to rhyolite composition, with the bulk composition characterized by a SiO_2 content of ~67 wt% (Fig. 9).

BOJ-03 – Twelve sanidine crystals from BOJ-03 provided a $^{40}Ar/^{39}Ar$ weighted mean age of 14.5±0.6 ka (2σ analytical uncertainty; Fig. 8). Although we found only a few fresh glass shards suitable for WDS-EMPA in this tephra, the composition shows a high variability, ranging from latite to trachyte (Fig. 9)**.** Laser ablation on twelve clinopyroxene crystals from BOJ-03 yielded a mean $^{87}Sr/^{86}Sr$ ratio of 0.70767±0.00157 (Table 3).

Site (fig.4)	Sample	Dating method			Tephra		Laboratory	Fault segment
		$^{40}Ar/^{39}Ar$	^{14}C AMS					
		age ka	Measured age BP	Calibrated age BP (2σ cal. 95%)	Volcanic source	Volcanic eruption		
T2	CCH-01		5350 ± 30	6270-6005			Beta Analytic	CDF
	CCH-02		2800 ± 30	2965-2845				
	CCH-03		2110 ± 30	2345-2160				
	CCH-04		2270 ± 30	2150-1995				
PAT-01		106 ± 1			Campania	X5, C27 TM25	LSCE	MPF
PAT-02		14.4 ± 0.4			Phlegrean Fields	NYT		
PAT-03		482 ± 3			Roccamonfina	Rio Rava		
SMAX-02		582 ± 1			Early Roccamonfina	Pre-Rio Rava		RF
BOJ-03		14.5 ± 0.4			Phlegrean Fields	NYT		CDF

Table 2. Laboratory ages of samples considered in this study. LSCE, Laboratoire des Sciences du Climat et de l'Environement, Gif-Sur-Yvette, France. $^{40}Ar/^{39}Ar$ ages are quoted at 2σ analytical uncertainty. AMS, accelerator mass spectrometry. 2σ calibration with software Calib 7.1, Stuiver et al., (2010).

Table 3. Sr isotope compositions determined by laser ablation inductively coupled plasma mass spectrometry (LA-ICP-MS) on clino-pyroxene crystals form the investigated Matese tephra. See Supplementary dataset DS3 for analytical details and instrument configuration.

SMAX-01 $^{87}Sr/^{86}Sr_{corrected}$	PAT-02 $^{87}Sr/^{86}Sr_{corrected}$	BOJ-03 $^{87}Sr/^{86}Sr_{corrected}$
0.7087	0.7087	0.7066
0.7097	0.7088	0.7062
0.7092	0.7077	0.7090
0.7094	0.7074	0.7073
0.7093	0.7093	0.7107
0.7097	0.7081	0.7063
0.7101	0.7087	0.7057
0.7085	0.7077	0.7076
0.7102	0.7084	0.7067
0.7100	0.7081	0.7052
0.7102	0.7087	0.7083
0.7093	0.7075	0.7085
0.7116		
Mean (±sd)	Mean (±sd)	Mean (±sd)
0.7097±0.0008	**0.7083±0.0006**	**0.7073±0016**

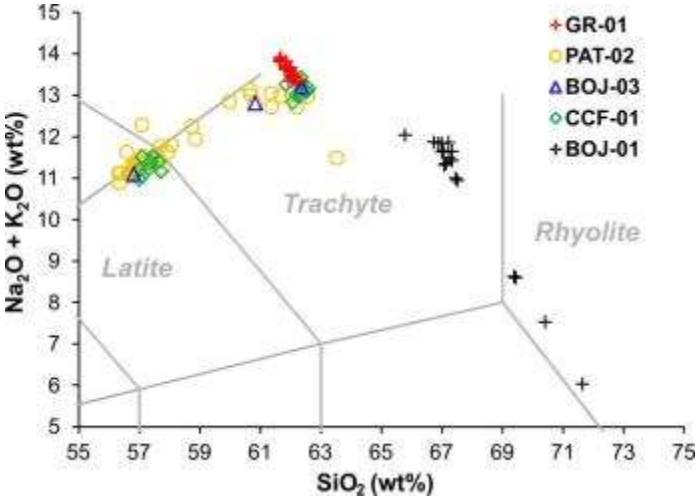

Fig. 9. Total alkali versus silica classification diagram (TAS, Le Maitre, 2002) for the Matese tephra (see Fig. 2 for sample location).

4.2. Structural data from the Northern Matese Fault System (NMFS)

4.2.1. ERT data

Results from the ERT investigations performed along the north-western prosecution of the BF segment (Fig. 2) show a subvertical, lateral contact between terrains with different resistivity values, which we interpreted as the tectonic limit between the Molise Flysch and the lacustrine infilling and that we termed Bojano buried fault (BBF, Fig. 10). Near the surface, this contact is sealed by higher resistivity terrains (ERT 2 in Fig. 10).

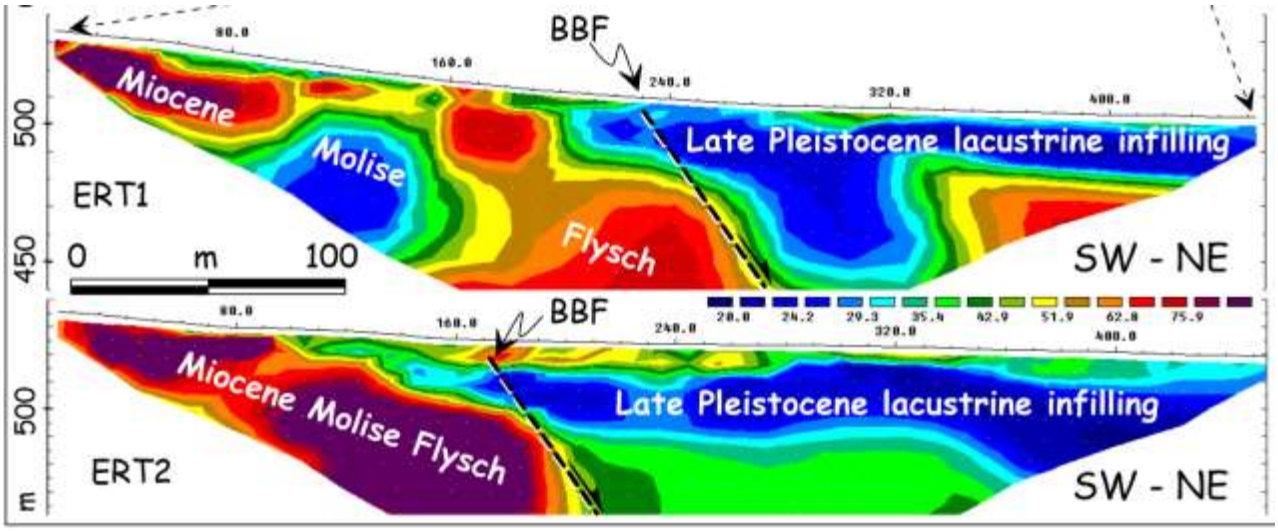

Fig. 10. Results of the ERT investigation performed along the Bojano buried fault (BBF; see location of the traces in Fig. 2).

4.2.1. Structural analysis

Main fault segments are aligned or arranged in a right stepping *en echelon* pattern, except the BF that is characterized by a northward 3-km step-over with respect to the adjacent CDF and RF. Moreover, the BF parallels the southern strand of the buried Bojano fault (BBF in Fig. 2), which we inferred from our ERT results (Fig. 10).

The equal-area, lower hemisphere projections of the fault planes and poles grouped for the single fault segments match strictly the average macroscopic trend of the five faults of the PFS (i.e., MPF, CMF, RF, BF, and CDF), with the last generation of *striae* being consistent with an overall NE-trending extension. All 125 structural stations are characterized by fault kinematics that is strictly consistent with almost pure normal faulting on planes generally trending ~N305° for the MPF, CMF, RF, and BF, whereas the general trend of CDF is N280° (Fig. 2). We measured slightly different orientations for both faults and *striae* at the tip of the macroscopic fault segments or along minor transfer faults (e.g. in Faure Walker et al., 2012).

The results of the pseudo-fault-plane solutions for both single segments and as the sum of all of them are shown in the left panel of Figure 11 (see methodological details in section 3.1.). Results indicate a strike of N313° and a dip of 65° for the MPF, a strike of N305° and a dip of 51° for CMF, a strike of N311° 64° for RF, N294° 73° for BF, and N280° 52° for CDF (Fig. 11, left panel). The pseudo-fault-plane solution of all the data provides a strike of N299° and a dip of 61° with a T-axis trending N35°15°.

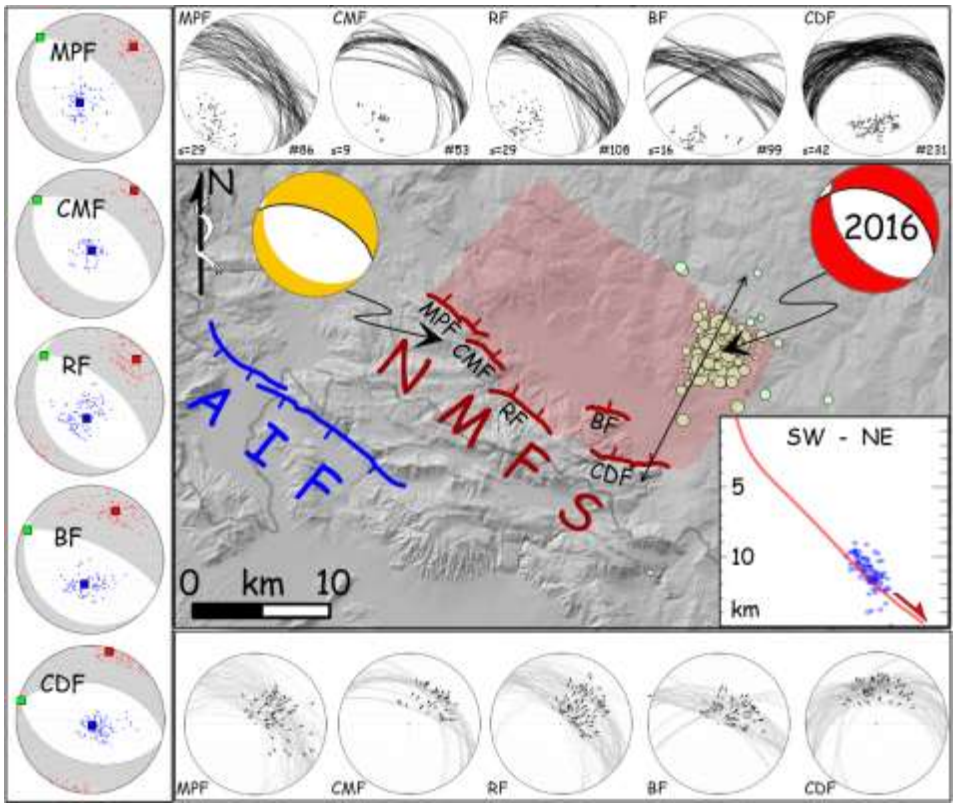

Fig. 11. Hypocentral distribution of the January 2016 seismic sequence (maximum Mw 4.4) and associated focal mechanism (QRCMT, 2016. Data from: http://iside.rm.ingv.it/ and courtesy of A. Basili, INGV, Rome). Orange beach-ball derives from the kinematic analyses of the geostructural data, i.e., pseudofault-plane solution using moment tensor axes (Allmendinger et al., 2012). The pink area roughly depicts the N-Matese fault plane at depth. Lateral panels, synopsis of the results of the geostructural analyses; upper panel, stereoplot of the geostructural stations located along the five main segments (lower hemisphere, fault planes and poles; s, number of stations, #, number of measures); lower panel, *striae* trend; left panel, pseudofault-plane solutions of each single fault segments, together with the S1 (blue), S2 (green), and S3 (red) axes. Note the strong matching between the pseudofault-plane solution and the 2016 fochal mechanism, both evidencing NE-SW extension (T-axes trending N35°15°, and N218°4°, respectively).

4.3. Paleoseismological analyses along the NMFS

Results of the high precision profiles (yellow lines in Fig. 7) evidence the presence of a net ~1-m-high ground step immediately uphill the underlying fault plane (Fig. 12), whereas some other results show also a couple of uphill retreated scarp edges (inflection points *sensu* Wallace, 1980; e.g. in Fig. 13).

Fig. 12. View looking south of a scarplet (~1.3 m high) along the Colle della Defenza fault which likely attests the 1805 surface faulting, as described by some historical sources. The cataclastic rocky fault plane outcrops just below the ground step.

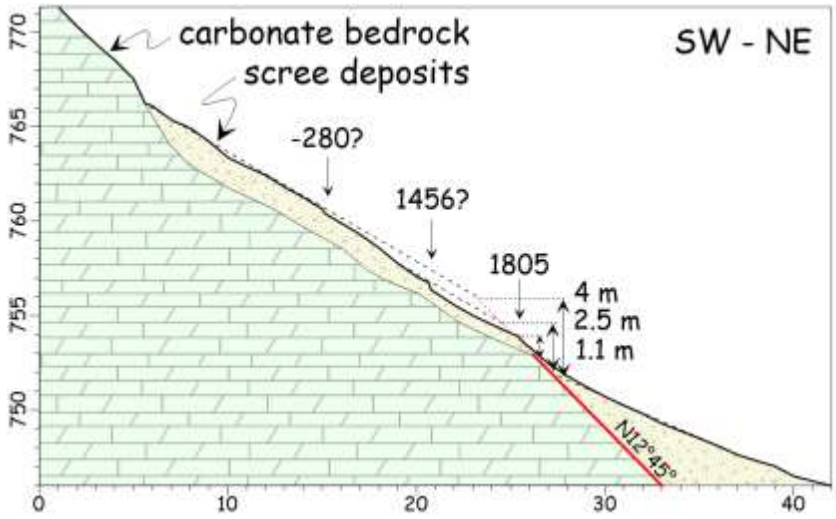

Fig. 13. High resolution topographic leveling (line 2 in Fig. 7) across the fault scarp of Colle della Defenza fault (m a.s.l.). This section suggests the occurrence of three surface faulting episodes that perturbed the natural profile of the slope. The three inflection points could be related to the main historical earthquakes with local epicenters (likely the early 3rd century BC, and the 1456 and 1805 events). The surface rupture for the 1805 earthquake (here 1.1 m high) is attested by coeval accounts.

Following this indication, we excavated a first paleoseismological trench along a 34°-dipping, alluvial cone, which is fed by an ephemeral creek. At this locality, the apex of this fan buries the fault plane, presenting a compound fault scarp aligned with the rock fault scarp that runs along the adjacent slope (Fig. 12). Regrettably, we could only exhume a massive, loose, coarse gravel unit, with up to 1-m-

sized boulders, dragged along a 45°-dipping N278° rock-fault plane, and a 10-cm-thick, green clayey fault-gouge, with striae indicating a 110° rake (i.e., right-lateral offset). Despite the unquestionable dragging and faulting of the fan alluvia, we did not find datable material or colluvial wedges to constrain paleoseismic events. Therefore, we excavated a second trench. This new trench offered more clues on the recent activity of the fault (T2 in Fig. 7). The trench was opened facing a N280° striking, 70° dipping slickenside, at the lateral limbs of two coalescing debris cones, in a gently dipping area (12°). The excavation was 8 m long and reached a depth of 3 m (Fig. 14). The fault footwall consists of highly fractured limestones, which are faulted against slope deposits and are mainly made of silty colluvia with fine gravels, reworked paleosols, and a lithon of thinly-laminated clayey flysch containing a carbonate boulder. Secondary fault-splays affect the entire sequence, with the exception of the uppermost layers exposed in the trench-wall.

Fig. 14. View of the fault zone in western wall of trench T2 (Fig. 8). The grey terrain at the bottom is a lithon of Molise Flysch dragged along the fault plane (white arrows). Net is 0.5 spaced. See Fig. 20 for interpretation.

Besides the along-fault dragged flysch wedge (unit 9 in Fig. 15) and its colluvium (8), the lowermost unit of the hanging wall is made of matrix-supported, fine angular gravels (6), with a stiff, tough yellowish silty-clayey matrix, which contains also sparse carbonate pebbles (up to 10-cm-sized). Unit 6 is both faulted against units 8-9 and unconformably layered over these units through an erosional

surface (es1). Toward the northern side of the trench, unit 6 is buried by dark, blackish clayey silts (5), with abundant cm-sized carbonate pebbles, mainly grouped in separate pockets, and strongly molded at the top by an erosional surface (es2). The upper part of the hanging wall mostly consists of pedogenized, brown-reddish, clayey-sandy silt, with sparse carbonate pebbles (4, 4b).

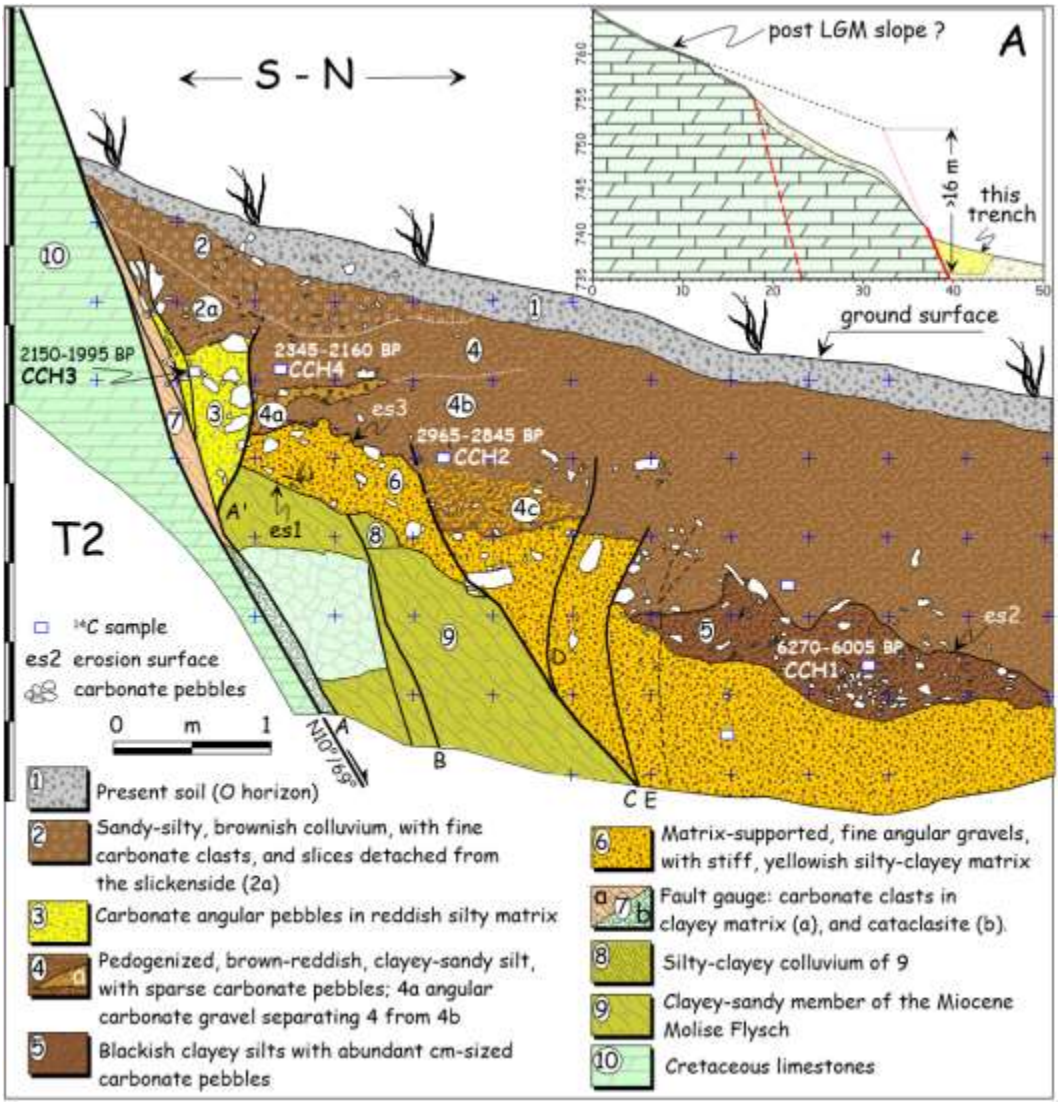

Fig. 15. Log of the western wall of trench T2 in Fig. 8. It is worth noting that all the hanging wall succession is faulted by the main fault and by the secondary splays, except units 1-2 which seal the ultimate offset. AMS ages are 2σ calibrated (see Tab.1). Basing on the high-resolution topographic profile carried out across the fault scarp and the trench axis (see Fig. 13 ; trace 3 in Fig. 7); here the post-LGM vertical offset likely exceed 16 m. See text for further details and paleoseismic interpretation.

Close to the main fault (A) and to the fault-splays (A', B, C), we identified different wedge-shaped bodies, which likely colluviated from the described deposits or from parent materials exposed above the trench site, in the fault footwall. For instance, unit 8 is entirely made of material derived from the

589 flysch unit 9. Sub-unit 4c derives from unit 6, with softy-pebbles of unit 6 being supported by a matrix
590 made of unit 4 material. Sub-unit 4a is an elongated wedge of angular carbonate gravel deriving
591 directly from the limestone slickenside. Unit 3 is a tectonic wedge filled by carbonate angular pebbles,
592 likely fallen from the limestone scarp, within reddish silty matrix. Units 2-2a are two superimposed
593 colluvial wedges made of material derived from the uppermost layers of unit 4, with fine carbonate
594 clasts and slices detached from the slickenside. Unit 7 consists of carbonate clasts in clayey matrix,
595 strongly dragged and packed between the main fault and the slope deposits. Unit 1 is instead the
596 present porous soil (horizon O) that is very rich in leaves and wooden material.
597 The age of the faulted deposits has been constrained by four AMS dating on bulk material (Tab. 2;
598 Fig. 15), as we did not find charred material in any units. We avoided to date the uppermost layers
599 that, due to its close proximity to the ground surface , was likely contaminated by younger carbon
600 (e.g. unit 2-2a). Considering the colluvial nature of almost all deposits, the dates we provide hereafter
601 do not necessarily represent the sedimentation age of the investigated layer, as a fraction of older
602 carbon may derive from the parent material from which the colluvial units were originated. All dates
603 indicate that the deposition and faulting of the hanging wall occurred in the very late Holocene; in
604 particular, unit 5 provided an age of 6270-6005 cal. BP (CCH-01), thus predating unit 6; the bottom
605 of sub-unit 4b provided an age of 2965-2845 cal. BP (CCH-02), thus predating sub-unit 4c; the bottom
606 of unit 4 provided an age of 2345-2160 cal. BP (CCH-04), thus predating sub-unit 4a; the tectonic
607 wedge labeled 3 provided an age of 2150-1995 cal. BP (CCH-03), which likely belongs to the
608 inherited matrix of unit 4, thus largely postdating sub-unit 2 and 2.
609
610 **5. Discussion**
611 ***5.1. Tephra age and correlation and chronology of Bojano Basin sedimentary infilling***
612 Based on the stratigraphic data and results from $^{40}Ar/^{39}Ar$ dating and previous geochronological data,
613 we here outline the chronological framework of the Bojano Basin sedimentary infilling. Additional
614 indirect geochronological constraints are provided by the correlation of the analyzed tephra with dated
615 proximal or distal counterparts via geochemical fingerprinting. To this end, since tephrochronology
616 can be relevant on a scale that goes well beyond the regional interest of this study (e.g. Lowe, 2011),
617 we also briefly discuss the potential correlation for the tephra that we dated through $^{40}Ar/^{39}Ar$ method.
618 **San Massimo terraced lacustrine – early Middle Pleistocene.** The base of the exposed San
619 Massimo terraced lacustrine deposits, firstly described by Brancaccio et al. (1979), was dated by Di
620 Bucci et al. (2005) at 621±6 ka and 649±21 ka. Our dating of the SMAX-01 tephra from the
621 uppermost interval of the same outcrop (582±1 ka; 2σ; analytical uncertainty; Fig. 8) confirms and
622 refines the chronology of this lacustrine unit. The age of SMAX-01 is similar within uncertainty to

623 the age obtained by Peretto et al. (2015) from a tephra sampled in the Lower Paleolithic site of Isernia
624 La Pineta, only 20 km northwest of our site (i.e., 586±1 ka, U4T pumice layer). The $^{87}Sr/^{86}Sr$ ratio of
625 0.7097±0.0008 (Table 3) we obtained for SMAX-01 tephra is consistent with the Roccamonfina pre-
626 caldera products measured by Conticelli et al. (2009; 0.7093-0.7100). This ratio fits also those of
627 tephra SL1 and SL2 from the Mercure basin (both with $^{87}Sr/^{86}Sr$ 0.7100. See location in Fig. 1, right
628 panel), which were dated as slightly antecedent 560 ka, and tentatively attributed to the early
629 Roccamonfina volcano by Giaccio et al. (2014). Therefore, considering the large grain sizes of
630 pumice of both levels (SMAX-02 and U4T), it is likely that they were sourced by the 40-km-far
631 Roccamonfina stratovolcano, the closest volcano located in a favorable position for both sites with
632 respect to the prevailing westerlies.
633 **Early slope-derived breccia – Middle Pleistocene**. The age we obtained for PAT-03 allows us to
634 ascribe the unconformably underlying deposits of the Early slope-derived breccia to the Middle
635 Pleistocene. The age of PAT-03 is close to the $^{40}Ar/^{39}Ar$ age obtained by Di Bucci et al. (2005) for a
636 tephra layer packed within a paleosol near Isernia, 7 km far away from this site (San9b, 476±10 ka).
637 Similarly to SMAX-02, the coarse grain-size of the pumice fall suggests a relatively proximal source,
638 and the Rio Rava stage of the Roccamonfina volcano (~440-550 ka, Rouchon et al., 2008) appears as
639 the most likely correlative for PAT-03. The intense explosive activity of this phase of the
640 Roccamonfina volcanic evolution is documented also in very distal settings, as for instance in the
641 Mercure basin (m in Fig. 1, right panel), where two out of nine Roccamonfina ash layers were dated
642 at 494±11 ka and 517±3 ka ($^{40}Ar/^{39}Ar$ age), being these layers isotopically (Sr) and chronologically
643 consistent with the Rio Rava stage (Giaccio et al. 2014).
644 **Inner basin Lacustrine-palustrine-fluvial deposits – Middle Pleistocene.** The major element
645 composition of the glass from BOJ-01 tephra matches the chemical composition of the glass from
646 MOL14 tephra (Fig. 16c) found by Amato et al. (2014) in core S2 (Fig. 2), 3 km west of the BOJ-01
647 site. Amato et al. (2014) correlated the MOL14 tephra with the MOL10 tephra, the latter occurring in
648 their S1 core and dated at 311±5 ka. As both MOL14 and MOL10 tephra were correlated with the
649 White Trachytic Tuff from the Roccamonfina volcano, also BOJ-01 can be conceivably attributed to
650 the same eruptive units. Therefore, the related interval of the Lacustrine-palustrine-fluvial deposits
651 can be dated as ~311±5 ka.
652 **Late slope-derived deposits – Late Pleistocene.** The layer PAT-01 (106±2 ka) and PAT-02
653 (14.4±0.4 ka) provide the lowermost and uppermost chronological boundaries for the Late slope-
654 derived deposits that can be thus dated as Late Pleistocene.
655 The age of PAT-01 precisely matches that of the POP3 tephra from the lacustrine Sulmona succession
656 (s in Fig. 1, right panel), located 90 km NW from this site, and correlated to the X-5 marine layer

(Giaccio et al., 2012; 106±1 ka). Therefore, although the lack of chemical data for PAT-01 prevents secure correlation, we can arguably propose that PAT-01 corresponds to the widespread X-5 layer, representing an important tephra marker for the Mediterranean MIS 5 paleoclimate studies (e.g. Regattieri et al., 2015).

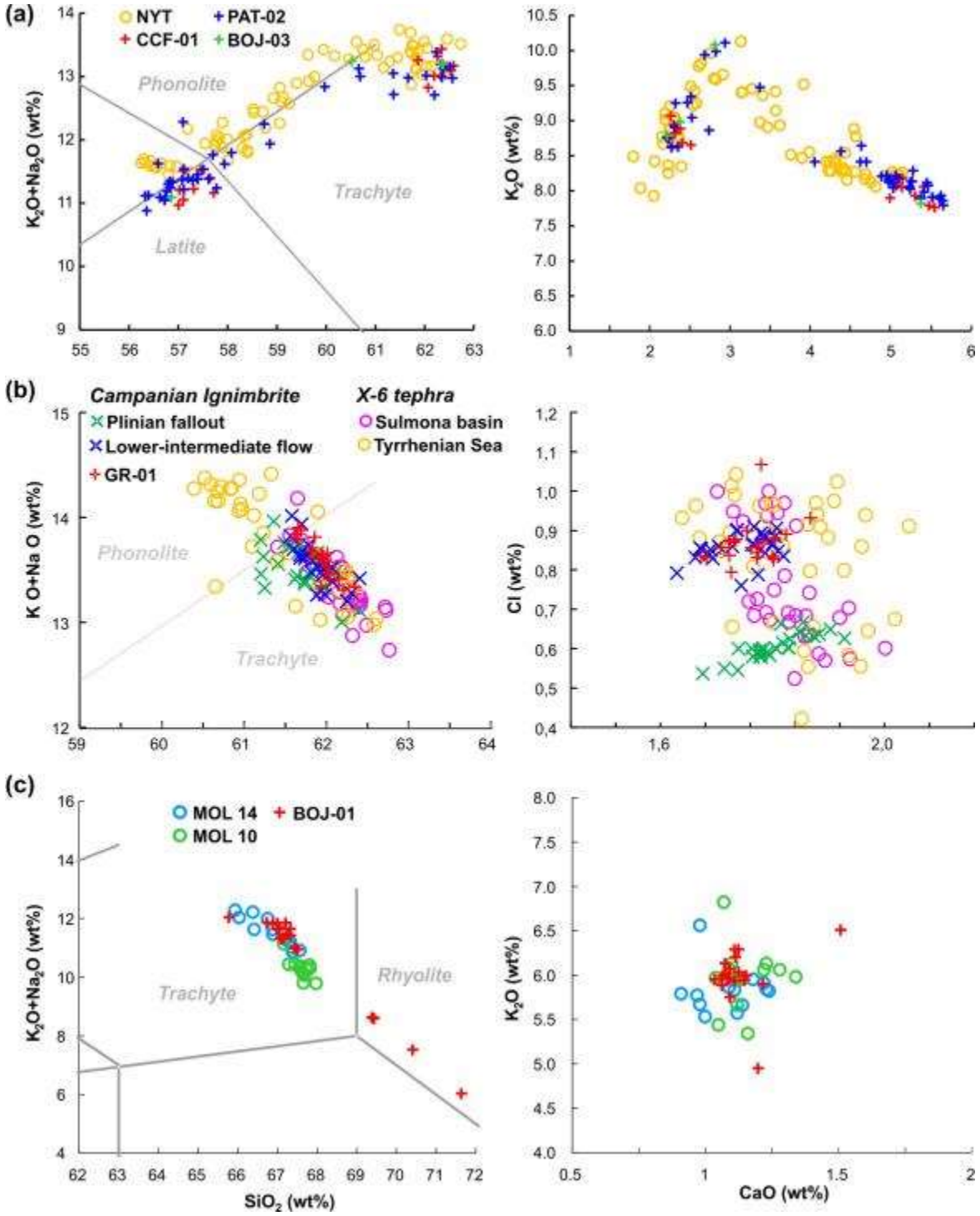

Fig. 16. Total alkali versus silica classification diagram (Le Maitre, 2002) and representative bi-plots for the Matese tephra PAT-02, BOJ-3 and CCF-01 (a), GR-01 (b) and BOJ-1 (c) compared with WDS-EMPA or SEM-EDS glass composition of their proximal or distal counterparts. Data source;

Neapolitan Yellow Tuff (NYT) proximal units: Tomlinson et al. (2012); Campanian Ignimbrite (CI) proximal Plinian fallout and lower-intermediate pyroclastic flows: Tomlinson et al. (2012); X-6 tephra from Sulmona basin and Tyrrhenian Sea: Giaccio et al. (2012), Iorio et al. (2014); MOL10 (311±5 ka) and MOL14 tephra, occurring in sedimentary succession of the Bojano Basin and correlated to the early stages of White Trachytic Tuff eruptions, dated between ~317 and ~300 ka (Giannetti and De Casa, 2000): Amato et al. (2014). All compositions are normalized to 100% ($Cl+F+SO_3$-free).

Both the glass chemical composition (Fig. 16a) and the age of the PAT-02 tephra match the products from the caldera forming Neapolitan Yellow Tuff eruption (NYT), occurred in the Campi Flegrei volcano and dated at 14.9±0.4 ka (2σ) by $^{40}Ar/^{39}Ar$ methods (Deino et al., 2004). Based on this very striking convergence of geochronological and geochemical data, PAT-02 can be unambiguously correlated to the NYT.

The composition of the third tephra found in the basal-middle interval of the Late slope-derived deposits matches the composition of the most evolved glass from both marine X-6 tephra (and equivalent mainland layers; e.g. Giaccio et al., 2012; Wulf et al., 2012; Iorio et al., 2014; Insinga et al., 2014), and from Campanian Ignimbrite (CI) (Fig. 16b) that is the largest eruption of the Campi Flegrei caldera (dated at ~39-40 ka; De Vivo et al., 2001). Although hardly distinguishable in the total alkali silica classification diagram, by using different discriminating diagrams, the composition of the GR-01 glass is closer to that of the CI than to that of the X-6, specifically to that of the lower-intermediate pyroclastic flow of the CI eruption (Tomlinson et al., 2012). Therefore, this tephra correlation provides a further chronological constraints to the Late slope-derived deposits of ~39-40 ka.

Late alluvial-fan deposits – Late Pleistocene. The $^{40}Ar/^{39}Ar$ weighted mean age of 14.5±0.6 ka (2σ analytical uncertainty; Fig. 8) for the tephra BOJ-03 allows us to ascribe the uppermost interval of the Late alluvial-fan deposits to the Late Glacial period. Furthermore, both age and chemical composition of BOJ-3 are virtually identical to PAT-02 and NYT (Fig. 16a), suggesting that this layer is correlated with both. This correlation is also supported by the $^{87}Sr/^{86}Sr$ ratio of 0.70767±0.00157 for BOJ-03, which is consistent with the ratio measured by Pappalardo et al. (2002; 0.70761-07756) for the NYT.

The correlation between PAT-02 and BOJ-03 allows us to join the two $^{40}Ar/^{39}Ar$ datasets to obtain a statistically improved age for both tephra and their proximal equivalent NYT. This yielded a weighted mean age of 14.5±0.4 ka (2σ, full propagated uncertainty; Fig. 8), which is the best and most robust $^{40}Ar/^{39}Ar$ age published so far for the NYT that is a very important Late Glacial regional extra-regional tephra marker (e.g. Lane et al., 2015).

Based on chemical composition, also the layer CCF-01 can confidentially correlated to the NYT (Fig. 16a), thus confirming the occurrence of this tephra in the uppermost interval of this unit as it was

703 previously hypothesized based on the stratigraphic position and lithological features of the tephra
704 (Amato et al., 2014). This is also consistent with results from previous radiocarbon dating of bones
705 and paleosols from the uppermost 10 m-thick interval of the Campochiaro fan succession, which
706 yielded ages ranging between >35 ka and ~11 ka (Guerrieri et al., 1999). On the whole, this unit can
707 be thus conceivably ascribed to the Late Pleistocene phase of alluvial fan growth, which is ubiquitous
708 in the entire Apennines (e.g., Frezzotti and Giraudi, 1992; Giraudi et al., 2011; Galli et al., 2015).
709 The NYT provides a *terminus ante quem* for the older Uma fan, which can thus be conceivably
710 ascribed to the same Late Pleistocene alluvial system. Specifically, by considering its relatively
711 notable thickness (up to 20 m in borehole S of Fig. 7), we can conservatively assume that this fan
712 temporally extends from the late Middle Plestocene-early Upper Pleistocene up to the Last Glacial
713 Maximum. Therefore, its top depositional surface may be roughly dated between 33 ka and 17 ka.
714

715 ***5.2. Middle-Upper Pleistocene sedimentary-tectonic evolution and slip rates of the NMFS***

716 The stratigraphic and chronological framework provided in the above section, coupled with the
717 structural and paleoseismological data, allowed us to outline the long term sedimentary-tectonic
718 evolution of the Bojano basin and the Quaternary activity of the NMFS.
719 The earliest stage of the basin evolution is characterized by the establishment of a lacustrine
720 environment testified by the *San Massimo Middle Pleistocene lacustrine deposits*, the uppermost and
721 most recent part of which has been here dated at ~582 ka. Although this time-interval was not reached
722 by the 160-m-deep borehole (S1 in Figs. 2 and 17), we can conceivably assume that the lacustrine
723 system extended to the whole basin, as shown by the data in the 900 m-deep borehole by Amato et
724 al. (2016; Sd in Fig. 2), including the subsurface of the present flood plain bounded by the BF and
725 BBF (Fig. 2). Therefore, obtaining a sedimentation rate of 0.45 mm/yr in the interval between tephra
726 dated 311 ka and 426 ka in borehole S1 (~50 m of clay and silt. See log in Figs. 5, 11), and
727 extrapolating this rate to the lower succession, we could hypothesize that the lacustrine deposits
728 coeval to SMAX-02 tephra should occur at 290 m a.s.l., in the hanging wall of the BBF, that is 520
729 m below the San Massimo Middle Pleistocene lacustrine deposit (810 m a.s.l.; Figs. 4, 17). Neglecting
730 sediment compaction and assuming that lake water depth did not exceed a few dozens of meters – as
731 the shallow water lithofacies of the S1 and S2 cores (Amato et al., 2014) and San Massimo sediments
732 clearly suggest – these 520 m are the maximum vertical offset of the BBF during the past half million
733 years, which would imply an average slip rate of ~0.9 mm/yr for this fault and/or nearby ones.
734

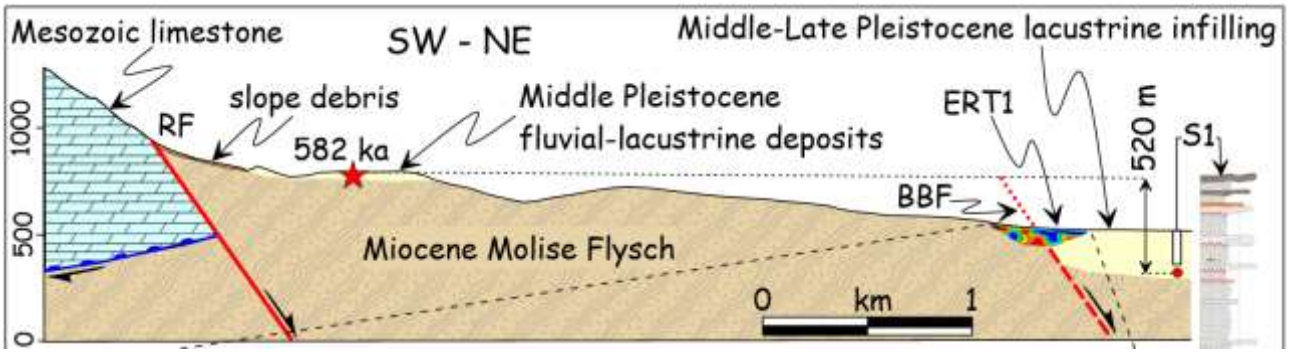

Fig. 17. Geological section (A-B in Fig. 2) showing the maximum possible offset (520 m) of the Middle Pleistocene lacustrine infilling of the Bojano basin across the buried Bojano fault (BBF). The red dot below borehole S1 is the inferred position of tephra SMAX-02 (~582 ka) in the hanging wall of the BBF (see text). The location of the buried fault has been defined by the two electrical resistivity tomographies carried out in this area (ERT1 and ERT2 in Fig. 2). Right, log of the 160-m-deep S1 borehole (a-b-c-d, clay-silt-sand-gravel) with the two dated tephra (from Amato et al., 2014). Bottom, ERT1 and ERT2; resistivity in ohm*m. Dashed line is the inferred BBF, separating the Miocene Molise Flysch terrains (higher resistivity values) to the lacustrine infilling (lower resistivity values). Note that ERTs are displayed at a greater scale (~ x10) than the geological section.

After this early stage (<582 ka), while the sector between PFS and BBF was definitively emerging, the lacustrine sedimentation persisted until the Holocene only in the hanging-wall of the BBF, i.e., below the present flood plain (Fig. 2). During the initial stages of this subsequent phase of the basin evolution, huge carbonate breccias (*Middle Pleistocene slope-derived breccias*) deposited along the whole PFS front (from MPF to CDF; Fig. 2), indicating a contemporary rejuvenation of topographic relief due to rapidly growing fault slopes (Fig. 6). The formation of slope-derived rudites ceased around or before the deposition of a pumice fallout from Roccamonfina Rio Rava stage, dated by us at ~482 ka (PAT-03).

Later, the Roccamonfina WTT tephra (~310 ka) deposited on both footwall and hanging-wall of the BBF (Fig. 18). The following fault movement of the BBF resulted in a total vertical offset of the lacustrine deposits containing WTT tephra on the order of only ~85 m (Fig. 18). This implies that, during the past 300 kyr, the slip rate of the BBF system reduced to ~0.3 mm/yr, which is significantly smaller than the ~0.9 mm/yr suggested for the last 580 kyr.

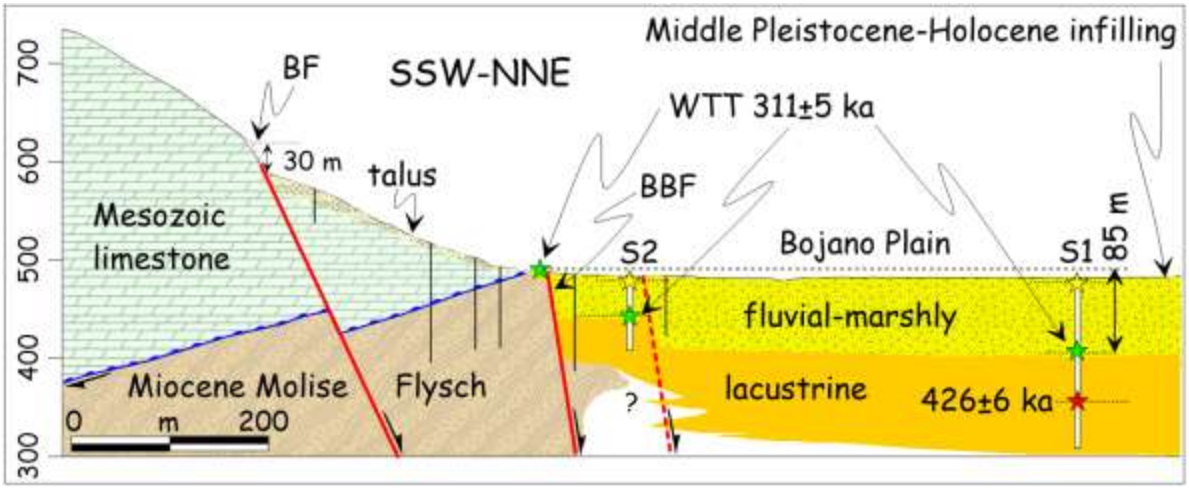

Fig. 18. Geological section (C-D in Fig. 2) showing the 85 m vertical offset of the fluvial-lacustrine level containing the White Trachytic Tuff (WTT) tephra (green stars) across the buried Bojano fault (BBF). S1 and S2 are boreholes in Amato et al. (2014; see Fig. 5), with an older tephra dated therein (red star), and the Neapolitan Yellow Tuff (yellow stars). Vertical bars, boreholes (after E.R.I.M., 1975). The section evidences also the 30-m-vertical separation of the slope surface across the Bojano fault (BF), and the negligible offset of the Neapolitan Yellow Tuff between S1 and S2.

Actually, if 85 m of vertical displacement occurred here in the past ~310 ka, we can conclude that the remaining 435 m (520 m minus 85 m; i.e., between horizons dated at 582 ka and 311 ka) took place in the preceding ~270 kyr, between 582 ka and 310 ka, implying a higher slip-rate of the BBF (>1.5 mm/yr) during that time span. On the whole, this is consistent with the mentioned huge production of syntectonic carbonate breccias before/around the Roccamonfina eruption of the Rio Rava stage dated at ~482 ka and the subsequent slowdown after this age. Indeed, after the deposition of this pumice fallout, which marks the interruption of breccias accumulation, the new onset of slope sedimentation happened only in the early Late Pleistocene, i.e., slightly before to the deposition of X-5 (PAT-01) tephra, dated by us at ~106 ka. This consideration implies a very long phase (more than 0.3 Ma) of no deposition and/or erosion, which suggest a substantial contemporaneous slowdown of the NMFS activity. Conversely, the formation of the ~50-m-thick debris-wedge in the hanging wall of the MPF during the Late Pleistocene, throughout the deposition of the PAT-01/X-5, CI, and NYT tephra, and the Holocene slope deposits (Fig. 19), implies a reactivation of PFS activity with a rough slip rate of ~0.5 mm/yr (i.e., 50 m/106 ka).

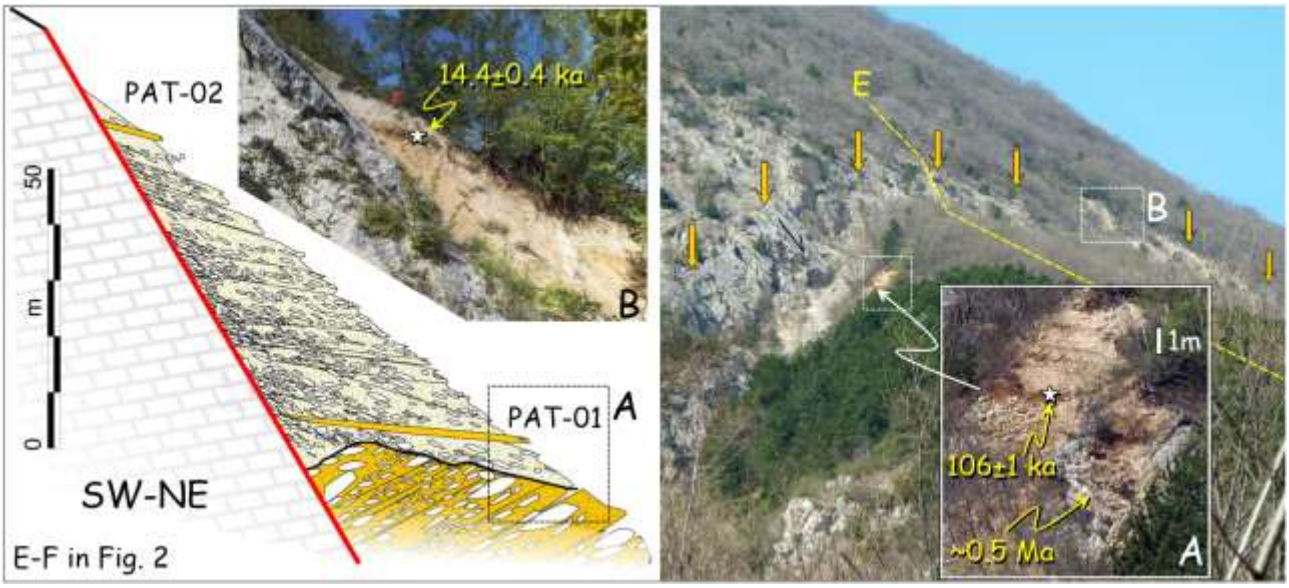

Fig. 19. Right, view looking west of the 20-30 m-high Mount Patalecchia bedrock-fault scarp (deep yellow arrows; see right panel in Fig. 4) and of the syntectonic Late Pleistocene slope-debris wedge. A, unconformity between highly tectonized Middle Pleistocene breccias (~0.5 Ma) and the early Late Pleistocene slope deposition. Left, sketch of the faulted slope succession, roughly matching E-F path in Fig. 2. B, uppermost part of the slope-wedge, with the faulted Holocene layers (person for scale). White stars in A and B are the X5 (PAT-01) and Neapolitan Yellow Tuff (PAT-02), respectively.

Unequivocal evidence of the recent activity of the MPF segment is provided by the tectonic deformation, which affects the topmost interval of this succession at site PAT-02 (Figs. 2, right panel of 19 and 20). At this locality, the described succession of Late Pleistocene-Holocene slope deposits lays over the bedrock fault scarp and is made of (*i*) coarse LGM gravels, (*ii*) barely reworked NYT tephra, and (*iii*) Holocene fine gravels and sands (Fig. 20). All these deposits are dragged and faulted by the N325°50° rock-fault plane with dip-slip striae, and are also offset by a synthetic splay cutting the hanging wall less than a dozen meters away from the main fault (Fig. 20). Across this splay, we measured 4 m of vertical throw of the NYT, which alone would imply a minimum vertical slip-rate of 0.3 mm/yr for the MPF. However, as the vertical separation of the slope profile that we measured here is 22 m (i.e., *nastro* height plus retreated fault scarp; inset A in Fig. 20), assuming a rough slope rectification during the strong LGM rhexistasy phases (e.g. see Dramis, 1983; Roberts and Michetti, 2004; Galli et al., 2012), and adding up also the thickness of the Holocene deposits and the splay offset, the slip rate of the MPF segment could be approximated to about 1 mm/yr in the past 30 kyr.

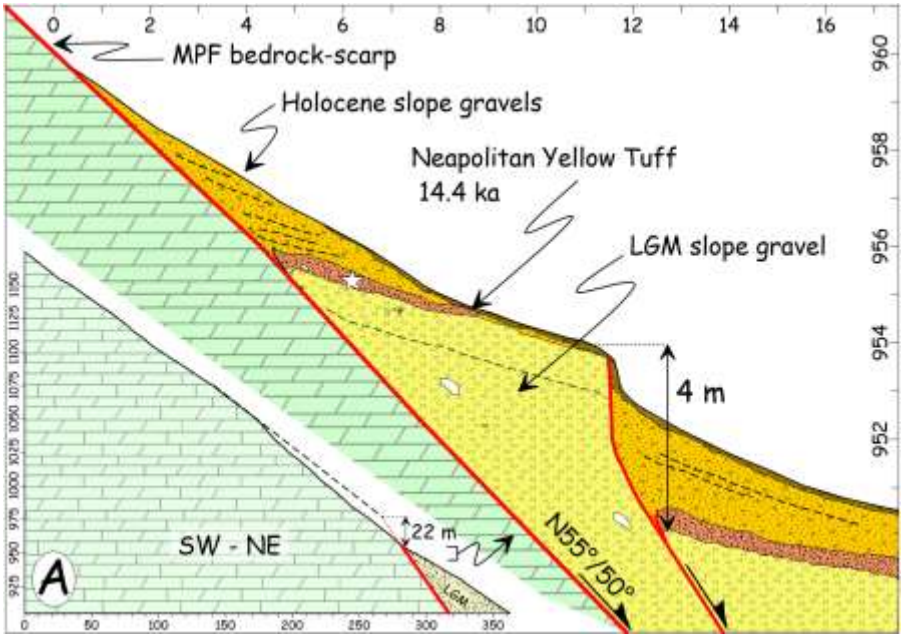

Fig. 20. Geological section of inset B site in Fig. 13 (m a.s.l.). The Last Glacial Maximum slope-gravel succession ends with a pedogenized level made at expense of a tephra (Neapolitan Yellow Tuff) dated here at 14.4 ka (PAT-02). The Holocene is condensed in the uppermost 2-m-thick deposit. Besides a vertical separation of ~22 m of the slope profile (see the topographic profile of Fig. 13 , the post-LGM total offset must be added to further 4 m occurred post NYT, which yields a vertical slip-rate ~1 mm/yr.

Finally, the Late Pleistocene activity of the PFS has been ascertained also along its eastern segment (i.e., the CDF; Fig. 2). Here the main branch of the CDF crosses the apex of the Uma fan (Fig. 20), resulting in the displacement of the LGM surface by at least 20 m (Fig. 21). Hence, since the LGM (25±8 ka), we can roughly calculate a vertical slip rate of ~0.9±0.3 mm/yr and 1.2 mm/yr (i.e., 20 m ÷ 25±8 ka).

5.3. Holocene and historical activity of the NMFS

The historical activity of the PFS was unambiguously documented by archeoseismological investigations of Galli et al. (2002) at the Hercules' sanctuary of Campochiaro (4th century BC-4th century AD), built on the surface of the Uma fan, straddling an oblique, secondary splay of the PFS (thinner red line in Fig. 7). Here Galli et al. (2002) recognized an impressive faulting of the peripheral wall of its *temenos* and of some of the sacred buildings around the temple, relating it to an unknown ancient earthquake.

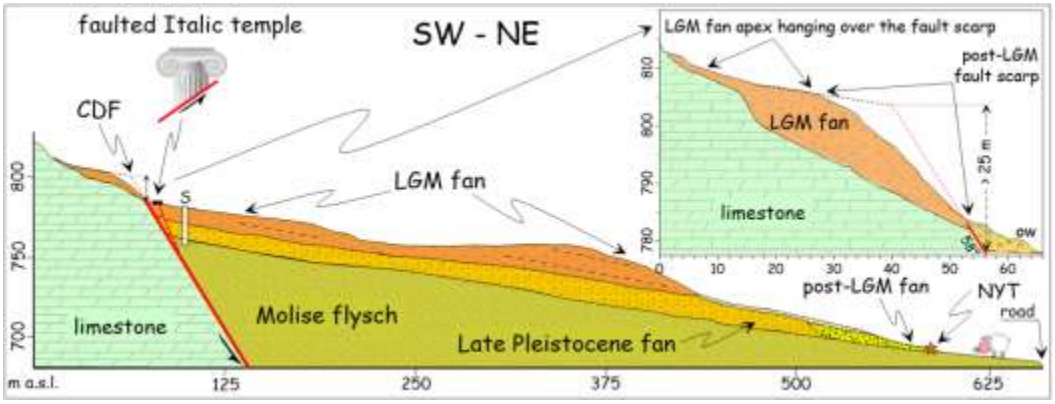

Fig. 21. Geological section (A-B in Fig. 7) along the Hercules' sanctuary alluvial fan, and across the Colle della Defenza Fault (CDF), evidencing the vertical offset of the Last Glacial Maximum (LGM) fan apex (s, projection of a borehole drilled in the sanctuary area). The section shows also the location of the Neapolitan Yellow Tuff tephra (NYT) at the bottom of the Holocene alluvial apron. Between the Miocene substratum (Molise Flysch) and the LGM fan a Late Pleistocene alluvial fan is likely present. The right panel is a detail of the fault zone, and contains one of the topographic leveling carried out across the CDF (yellow line 1 in Fig. 8) that allowed us to measure the vertical separation of the LGM fan surface (ow, current outwash gravels).

The very recent activity of the CDF is also suggested by the high precision profiles preparatory to the paleoseismological trenches (Fig. 13; see traces in Fig. 7). The total vertical separation of the uppermost inflection point ranges between 2.8 and 4.0 m, which should thus account for three surface faulting events, each one with an offset of 0.9-1.3 m (Fig. 13). The lowermost 1-m-high step (Figs. 12 and 13) can be reasonably associated to the last Mw 6.6 earthquake of the area, i.e. the July 26, 1805 event. According to historical accounts, chasms opened in this area (Pepe, 1806), and along these chasms "*the ground surface raised up to seven palms* (i.e., 1.8 m) .... *as happened near Guardiaregia, where a very long rupture opened in the rocky foothill*" (Poli, 1806).

Finally, the most compelling evidence of activity of the Holocene-historical activity of CDF hav been revealed by the paleoseismological analyses carried out in the present study. The detailed trench field logging and interpretation, supported by hundreds of photographs shot on different days and with different light conditions (both natural and artificial), coupled with structural analysis of wedges, and the time-spans bracketed by the AMS ages, all together provide evidence for several surface faulting events (EQ) that occurred in the late Holocene. In detail (see Fig. 15), the oldest visible earthquake (EQ1) occurred before the deposition of unit 6, when unit 9 was displaced by fault B, thus generating a scarp-related colluvial wedge (CW 8), which is entirely composed of flysch-derived deposits. Both units 9 and 8 were successively truncated by an erosional surface (es1) and sealed by the overlying unit 6. During/after the deposition of unit 6, faults A and C offset units 9-6 (EQ2), inducing the formation of a scarp-related CW (4c). This CW developed at the expense of unit 6 material fallen from fault C footwall, which therefore presents an erosional surface between faults A'-C. Then, fault

A and associated splays C-D-E cut through sub-units 4c-4b (EQ3), inducing the formation of another scarp-related CW (4a). All these units are faulted again (EQ4) by fault A-A', causing the formation of an open chasm filled by wedge 3 and sealed by the overlying CW 2a. A last event (EQ5) on fault A displaced all the sequence, including units 3-2a. The fault was then sealed by the CW 2.

EQ1 is not defined, as we only know that it occurred well before 6270-6005 BP. In turn, EQ2 occurred just prior than 2965-2854 BP, whereas EQ3 is much more defined, as it ruptured a considerable time after 2965-2845 BP and shortly prior than 2345-2160 BP (i.e., before 395-210 BC). Then, EQ4 happened at an undefined time after 2150-1995 BP (i.e., after 200-45 BC), EQ5 should, in turn, be really recent, CW 2 being right below the presently forming soil.

We are therefore confident that at least the three youngest events occurred in historical times: the oldest one just prior than 4^{th}-3^{rd} Centuries BC, the youngest one very recently (e.g., 1805 earthquake), and the intermediate one during an undefined period in between the oldest and youngest ones.

5.4. Spatial and temporal evolution of the NMFS

Our results highlight a differential distribution of the tectonic activity along different fault segments over time, with an overall slowing down of the buried Bojano faults with respect to the Piedmont fault system. Firstly, we recognized the evidence of a strong extensional tectonics during the late Middle Pleistocene time – reasonably post 580 ka and well before 310 ka – which was associated to high normal fault slip rates. For this time-span, there are robust lines of evidence for ≥ 1.5 mm/yr vertical slip rates on the buried Bojano faults (BBF in Fig. 2), which caused the downthrowing of the present Bojano plain sector (Figs. 17 and 18). This process implied a consequent regional rejuvenation that triggered the high production of coarse syntectonic carbonate breccias (~480 ka) piled all along the northern Matese slopes (e.g. in Fig. 6; Fig. 3 in Galli et al., 2002). Indeed, we dated remnant paleolake deposits predating this phase outcropping at more than 300 m above the present Bojano plain, containing early Roccamonfina volcano pyroclasts dated at 582 ka, whereas other key levels, that were previously dated across the BBF (e.g., Roccamonfina WTT tephra, 311 ka in Amato et al., 2014), indicate that this fault slowed down dramatically to ~0.3 mm/yr since 300 ka. This conclusion is supported also by the lithofacies of the cores described in Amato et al. (2014), accounting for a noticeable change in the sedimentary environments, switching from lacustrine-palustrine (~500-300 ka) to fluvial-marshy (300 ka to Present), which suggest a progressive drop of the volume accommodated by the BBF activity over time.

Stratigraphical and geochronological data indicate that, during the ~480-110 ka interval, the fault segments running along the flanks of the Matese carbonate massif (i.e., the PFS) also underwent a substantial slow-down of their tectonic activity. On the other hand, our data accounts for a strong

activity of the PFS during the Late Pleistocene, with vertical slip rates ranging between 0.5 and 1 mm/yr, and net slip rates even exceeding this maximum value. The faulting of the syntectonic debris wedge, which unconformably piled up in the MPF and CDF hanging wall between 106 ka and the Present, coupled to the height of the rock fault scarps along the slopes (e.g., 20-30 m of vertical separation; Figs. 17 and 18), and the offset of Last Glacial Maximum alluvial fans (Fig. 19), provided clear evidence for this prominent and sustained tectonic activity along the PFS. These slip rates are consistent with the GPS-deduced extension of this region, currently estimated at 1.6 mm/yr (Ferranti et al., 2015).

Conversely, the latest certain chronological markers investigated across the BBF (i.e., NYT tephra found in boreholes by Amato et al., 2014) show a negligible vertical separation, suggesting that the fault was almost or even definitely blocked before the Holocene. This fact is consistent with the information provided by the historical accounts regarding the local 1805 and 1456 Mw>6.5 earthquakes, for which there is no mention of opening of any coseismic fissure in the flat area occupied by the Bojano village (Porfido et al., 2002), i.e. the area crossed by the BBF (Fig. 2).

5.5. Paleoearthquake recurrence and seismotectonic implications

As far as the most recent activity of the NMFS is concerned our paleoseismological results (trench T2 in Fig. 7) account for four surface faulting events that occurred in the last 3 kyr (and at least another one prior to 6 ka), three of which during historical times. Fault length (28 km) and inferred offset per event (0.9-1.3 m) suggest that the magnitude associated to these events was ~Mw 6.7 (Wells and Coppersmith, 1994; Galli et al., 2008b). Therefore, in addition to cross-checking our results to other published data, we have to compare these results with the historical seismicity of the Bojano basin, both in terms of highest intensity datapoints distribution (HIDD) and of written sources eventually accounting for the formation of surficial breaks. Firstly, it is helpful remembering that the last three events defined in trench T2 (EQ3-5) occurred, respectively: shortly prior than 395-210 BC (EQ3); at an undefined time after 200-45 BC (EQ4); and in very recent times (EQ5) later than EQ4,

According to the archeoseismological results published by Galli and Galadini (2003), the fault investigated in trench T1 (Figs. 2 and 7) ruptured repeatedly in historical times. The first time in 280 BC, and likely twice after the 4th century AD (Fig. 22). In turn, according to data published by Blumetti et al. (2000) from a trench excavated across the MPF (TB in Fig. 2), one faulting episode occurred shortly after 2790-2490 BP (i.e., 845-540 BC), whereas at least another one happened successively. By comparing these three, independent results, we can conclude that the entire NMFS ruptured in the second half of the 1st millennium BC (between 845-540 BC and 395-210 BC), precisely in 280 BC (EQ3 in T2; see Fig. 22).

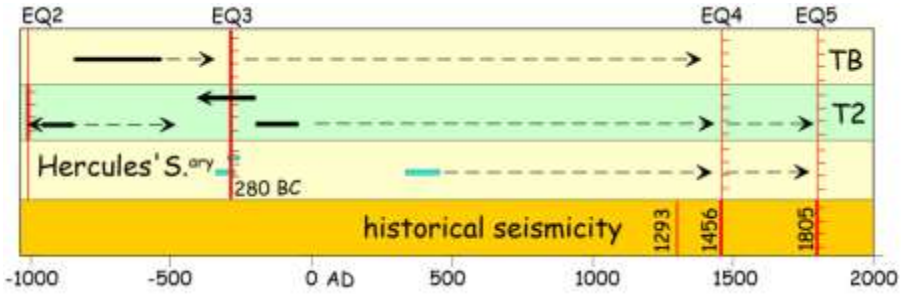

Fig 22. Chronogram of the surface rupture events (red barbed lines; bold where certain) identified from within trenches (TB, Blumetti et al., 1990; T2, this paper), Hercules' Sanctuary and historical accounts. Black rectangles, 2σ calibrated interval of key radiocarbon samples (arrow indicates *post/ante quem* term; dashed indefinite *post quem* term). Cyan rectangles, *post/ante/ad quem* terms provided by pottery shards and coins.

From our results, we know that the fault ruptured again twice after the 4th century AD, and this obviously caused destructive earthquakes in the Bojano basin. Therefore, if we compare the HIDD of the known strongest earthquakes of the area with the NMFS attitude, we could make some inferences concerning the two remaining paleoearthquakes (EQ4-5) observed in trenches. Figure 23 offers the easy solution to this question, as both the Mw 7.0, 1456 earthquake and its minor twin event in 1805 (Mw 6.6) exhibit a HIDD matching the NMFS hanging wall. Conversely, the 1688, Mw 7.0 event falls entirely outside the area subtended by NMFS, matching instead the southern sector of the composite 1456 HIDD. Moreover, as mentioned previously, while we do not have conclusive information concerning the 1456 earthquake[1], the 1805 coeval accounts document the opening of surficial breaks both along the antithetic faults of the NMFS, and along the Bojano and Colle delle Defenza fault segments, with indication even on the surface offset amount (e.g., up to a maximum displacement of 1.8 m; Poli, 1806).

Summarizing, we can reasonably assess that the NMFS sourced three Mw≥6.6 earthquakes in 280 BC, in 1456, and in 1805, as well as another one in the early 3rd millennium BP, i.e., just before 2965-2854 BP. This implies a recurrence time for this class of magnitude earthquakes of ~0.9 kyr in the late Holocene, despite through events irregularly spaced in time (e.g., between 0.35-1.75 kyr), as observed also for other primary seismogenic faults in the central Apennines (i.e., Fucino fault system: Galli et al., 2016; Upper Aterno fault system: Galli et al., 2011), southern Apennines (Mount Marzano fault system: Galli and Peronace, 2014; Aquae Iuliae fault: Galli and Naso, 2009), and Calabria (Lakes fault: Galli and Scionti, 2006; Cittanova fault: Galli and Peronace, 2015).

[1] According to Manetti (1457) the village of Bojano was submerged by waters which formed a lake: *" totum aquis undique circumdantibus obrutum*". This phenomenon could be explained by the coseismic upraise of the aquifer confined in the Bojano fault footwall, and by the sudden increase of water discharge of the Biferno river springs inside Bojano. The same occurred for the 1805 earthquake, as described by Poli (1806).

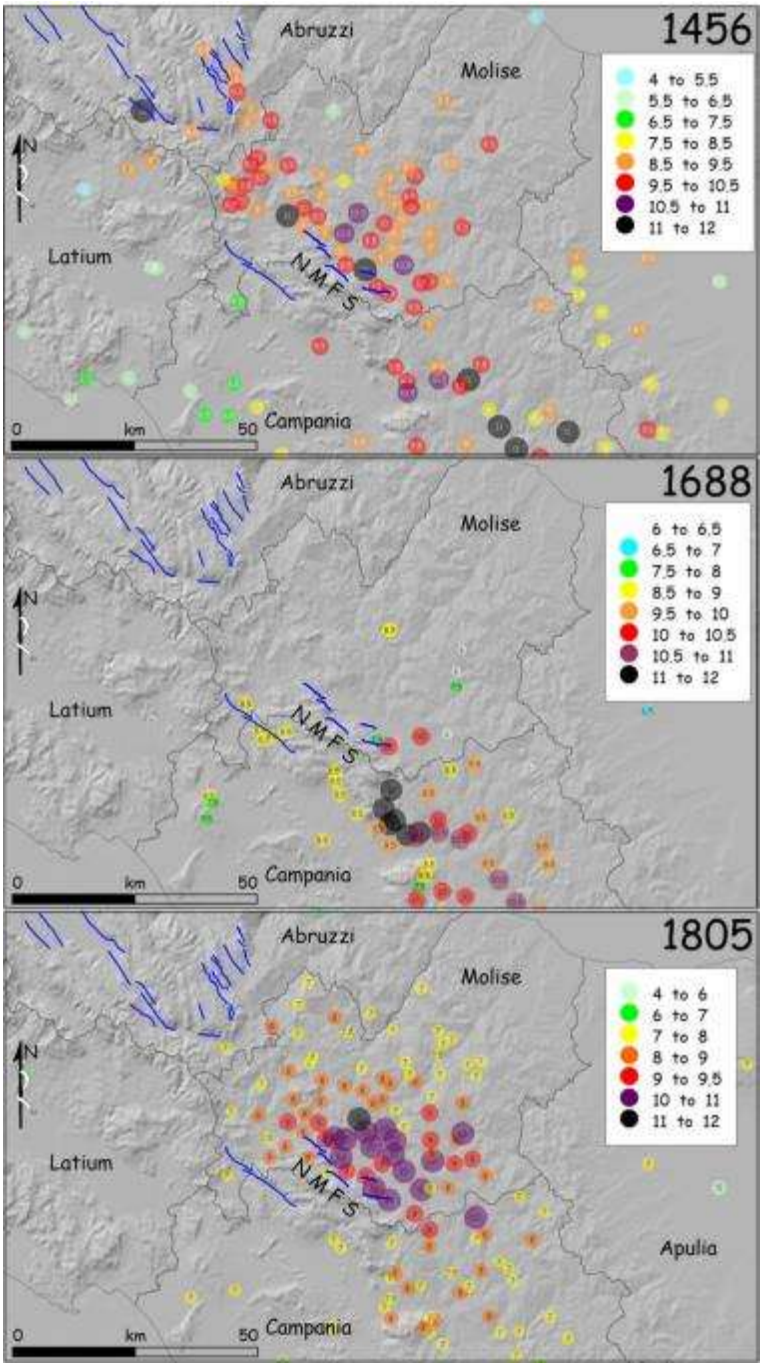

Fig. 23. Highest Intensity Datapoints Distribution (HIDD) of the three strongest earthquakes on record in the investigated area (1456 and 1688: unpublished report of P. Galli and D. Molin; 1805 from Esposito et al., 1992), compared to the attitude of the Northern Matese Faults System (NMFS) and of other known active faults (from Galli et al., 2008b). Note that the 1688 and the 1805 HIDDs together match the central-southern cluster of the 1456 HIDD, whereas the 1805 and the central 1456 HIDD fit the NMFS hanging wall.

Finally, the ongoing activity of the NMFS has been confirmed by a seismic swarm that took place in January 2016, when two hundreds <Mw 3 earthquakes following a Mw 4.4 mainshock occurred in the southern hanging wall of the NMFS, at ~10-13 km of depth. The focal mechanism of the mainshock (QRCMT, 2016; Fig. 1) and the preliminary hypocentral distribution (S. Barba and A.

Basili, pers. comm.) both evidence normal slip on a N295° fault plane, dipping ~45° NE, which fully matches the pseudo-fault-plane solutions obtained from the structural data collected along the fault segments. This implies that either a small patch of the SE-tip of the BF or, likely, of the NW-tip of the CDF might have ruptured at about 10 km depth (Fig. 11).

6. Concluding remarks

We have carried out an integrated study of the Bojano basin through stratigraphical, structural, geomorphological, geophysical, geochronological and paleoseismological analyses. The collection of this large and multidisciplinary dataset allowed the definition of the activity of the North Matese Fault System (NMFS) in the light of both long term tectonic-sedimentary evolution of the Quaternary basin and of its recent coseismic surface ruptures. Our results support an uneven rate of tectonic deformation for the fault segments composing the ~28 km-long N-Matese fault system over time. As a matter of fact, after a strong tectonic activity occurred around and after ~580 ka along the presently buried fault segments bounding the Bojano plain (BBF in Fig. 2), since at least 310 ka, slip rates progressively decreased, dying out during the Late Glacial-Holocene. Conversely, the piedmont fault system, running parallel to the northern Matese flanks (i.e., MPF, CMF, RF, BF, CDF segments in Fig. 2), appears to have undergone a similar slowdown of its activity during the 480-110 ka time span, to then restart, with a consistent slip rate >0.5 mm/yr and up to >1 mm/yr, at least for the last 110 kyr. Indeed, the evidence of post-Late Glacial activity and Holocene-historical coseismic surface ruptures are evident on both the outer segments of the NMFS, (i.e., MPF and CDF), and specifically on the CDF, where four Mw≥6.6 earthquakes have been paleoseismologically recognized and ^{14}C dated since 3 ka, including the historical 280 BC, 1456 and 1805 events. This result highlights that the NMFS - as well as other primary structures in the central Apennines - is one of the most hazardous seismogenic structures of Europe, capable of sourcing Mw>6.6 earthquakes every few centuries.

The multi-analytical and integrative approach was decisive for reaching our goals. In this methodological perspective, tephrochronology – and particularly the $^{40}Ar/^{39}Ar$ dating method – was essential. We have demonstrated a high reproducibility of the $^{40}Ar/^{39}Ar$ dating also for relatively recent tephra (e.g. the NYT of 14.5 ka), as well as the notable consistency between $^{40}Ar/^{39}Ar$ ages and glass composition of the tephra, highlighting the high accuracy and reliability of the chronological data acquired through this combined method. In the light of the conspicuous occurrence of pyroclastics in the Mediterranean, an enhanced application of this method could in the future become a key tool for improving our knowledge of the active tectonics of this region as well as of any other Quaternary evolutionary process, whose accurate dating is the fundamental prerequisite to their thorough understanding.

Acknowledgments

The views and conclusions contained in this paper are those of the authors and should not be interpreted as necessarily representing official policies, either expressed or implied, of the Italian Government. We are grateful to the municipality and to the Major of Campochiaro for the logistic support, to M. Iezza for excavating the trenches in such a difficult site. This study was carried out within the DPC-INGV-S1 Project "Base-knowledge improvement for assessing the seismogenic potential of Italy" founded by the Department of Civil Protection of the Presidency of the Council of Ministers of Italy. Non ringraziamo i Revisori? Meglio ringraziarli ora!

References

Allmendinger, R.W., Cardozo, N., Fisher, D., 2012. Structural Geology Algorithms: Vectors and Tensors. Cambridge University Press, Cambridge.

Amato, V., Aucelli, P.P.C., Cesarano, M., Jicha, B., Lebreton, V., Orain, R., Pappone, G., Petrosino, P., and Russo Ermolli, E., 2014. Quaternary evolution of the largest intermontane basin of the Molise Apennine (central-southern Italy). Rend. Fis. Acc. Lincei 25, S197-S216.

Amato, V., Aucelli, P.P.C., Cesarano, M., Cifelli, F., Leone, N., Mattei, M., Russo Ermolli, E., Petrosino, P., Rosskopf, C.M., 2016. The infill timing of a quaternary intermontane basin: new chrono-stratigraphic and palaeoenvironmental data by a 900 m deep borehole from Campochiaro (central-southern Apennine, Italy). Abstract to EGU General Assembly 2016.

Ballini, A., Barberi, F., Laurenzi, M.A., Mezzetti, F., Villa, I., 1989. Nuovi dati sulla stratigrafia del vulcano di Roccamonfina. Boll. G.N.V. 2, 533-555.

Ballini, A., Barberi, F., Laurenzi, M.A., Mezzetti, F., Oddone, M., Villa, I.M., 1991. Chrono-stratigraphy of Roccamonfina Volcanic Complex. Plinius 4, 35–36.

Bernabini, M., Eva, C., Nicolich, R., Baranello, S., Cercato, M., De Ferrari, R., Ferretti, G., Pellegrino, P., Scapillati, N., 2009. Microzonazione sismica del comune di Bojano (CB). Abst. Vol. GNGTS 2009, 262–265.

Blumetti, A.M., Caciagli, M., Di Bucci, D., Guerrieri, L., Michetti, A.M., Naso, G., 2000. Evidenze di fagliazione superficiale olocenica nel bacino di Bojano (Molise). Extended abstracts of the 19° GNGTS congress, Rome 7-9 November, Cd-rom, ISBN 88-900-385-4-3, 9 pp.

Bosi, C., 1975. Osservazioni preliminari su faglie probabilmente attive nell'Appennino centrale. Boll. Soc. Geol. It., 94, 827-859.

Bosi V., Galadini F., Galli P., Giuliani R., Meghraoui M., Messina P., Molin D., Stucchi M., 1997. La definizione di schemi strutturali per finalità sismotettoniche. In: riassunti del convegno AIQUA, Associazione italiana per lo studio del Quaternario; "Tettonica quaternaria del territorio italiano: conoscenze, problemi ed applicazioni", Parma, 25-27 febbraio 1997, 53.

Bousquet J.C., Grellet B., and Sauret B., 1993. Neotectonic setting of the Benevento area: comparison with the epicentral zone of the Irpinia earthquake. Annali di Geofisica, 36, 245-251.

Brancaccio, L., Cinque, A., Sgrosso, I., 1978. L'analisi morfologica dei versanti come strumento per la ricostruzione degli eventi neotettonici. Mem. Soc. Geol. It. 19, 621-626.

Brancaccio, L., Cinque, A., Orsi, G., Pece, R., Rolandi, G., Sgrosso, I., 1979. Lembi residui di sedimenti lacustri pleistocenici sospesi sul versante settentrionale del Matese, presso San Massimo. Boll. Soc. Nat. Nap. 88, 275-286.

Caiazzo C., Ascione A., Cinque A., 2006. Late Tertiary–Quaternary tectonics of the Southern Apennines (Italy): New evidences from the Tyrrhenian slope. Tectonophysics, 421, 23-51.

Calabrò, R., Corrado, S., Di Bucci, D., Robustini, P., Tornaghi, M., 2003. Thin-skinned vs. thick-skinned tectonics in the Matese Massif, Central–Southern Apennines (Italy). Tectonophysics 377 (2003), 269-297.

Capini, S., Galli, P., 2003. I terremoti in Molise. In: De Benedittis, R., Di Niro, A., Di Tommaso, D., Muccilli, O., (eds.). Dal 280 A.C. al 31 ottobre 2002 – I terremoti in Molise, Guida alla mostra, Ministero per i Beni e le Attività Culturali, Campobasso, 47 pp.

Castelli, V., 1993. A cluster of earthquakes in the Apennines at the end of the XIII century. Terra Nova, 5, 496-502.

Cinque, A., Patacca, E., Scandone, P., Tozzi, M., 1993. Quaternary kinematic evolution of the Southern Apennenes. Relationships between surface geological features and deep lithospheric structures. Annali di Geofisica 36, 249-260.

Conticelli S, Marchionni S, Rosa D, et al. 2009. Shoshonite and subalkaline magmas from an ultrapotassic volcano: Sr–Nd–Pb isotope data on the Roccamonfina volcanic rocks, Roman Magmatic Province, Southern Italy. Contributions to Mineralogy and Petrology 157, 41–63.

D'Agostino, N., Jackson, J.A., Dramis, F., Funiciello, R., 2001. Interactions between mantle upwelling, drainage evolution and active normal faulting: an example from the Central Apennines (Italy),). Geophys. J. Int. 147, 475–497.

D'Agostino, N., Avallone, A., Cheloni, D., D'Anastasio, E., Mantenuto, S., Selvaggi, G., 2008. Active tectonics of the Adriatic region from GPS and earthquake slip vectors. Journal of Geophysical Research 113, B12413.

D'Agostino, N., England, P., Hunstad, I., Selvaggi, G., 2014. Gravitational potential energy and active deformation in the Apennines. EarthPlanet. Sci. 397, 121–132.

D'Argenio, B., Pescatore, T., Scandone, P., 1973. Schema geologico dell' Appennino meridionale. Atti del Convegno: Moderne vedute sulla geologia dell'Appennino. Accad. Naz. dei Lincei, Quad. 183, 49-72.

D'Onofrio, A., 1805. Lettera ad un Amico in Provincia Sul Tremuoto Accaduto a 2 Luglio e Seguito Dall'Eruzione Vesuviana de 12 Agosto del Corrente 1805, Napoli.

Deino, A.L., Orsi, G., De Vita, S., Piochi, M., 2004. The age of the Neapolitan Yellow Tuff caldera-forming eruption (Campi Flegrei caldera-Italy) assessed by $^{40}Ar/^{39}Ar$ dating method. Journal of Volcanology and Geothermal Research 133, 157-170.

Di Bucci, D., Corrado, S., Naso, G., Villa, I., 2005. Growth, interaction and seismogenic potential of coupled active normal faults (Isernia Basin, central-southern Italy). Terra Nova 17, 44-55.

Doglioni, C., 1991. A proposal for the kinematic modelling of W dipping subductions: possible applications to the Tyrrhenian–Apennines system. Terra Nova 3, 423–434.

Doglioni, C., Mongelli, F. Pieri, P., 1994. The Puglia uplift (SE Italy): an anomaly in the foreland of the Apenninic subduction due to buckling of a thick continental lithosphere. Tectonics 13, 1309–1321.

Dramis F., 1983. Morfogenesi di versante nel Pleistocene superiore in Italia: idepositi detritici stratificati. Geogr. Fis. Din. Quat., 6, 180-182.

Duca della Torre, 1805. Notizie ricavate, ed osservazioni fatte in Contado di Molise, e precisamente in Bojano dopo il Tremuoto de' 26 di Luglio 1805. Archivio comunale di Bojano.

E.R.I.M., 1975. Sintesi delle indagini eseguite alle sorgenti del Biferno. Ente Risorse Idriche del Molise, Cassa per il Mezzogiorno, Ripartizione Progetti Idrici – Divisione IV, Campobasso.

Esposito, E., Luongo, G., Marturano, A., Porfido, S., 1987. Il terremoto di S. Anna del 26 luglio 1805. Mem. Soc. Geol. It. 37, 171-191.

Esposito, E., Laurelli, L., Porfido, S., 1992. Il terremoto del 26 luglio 1805. Lo scenario dei danni nella citta di Isernia. In: Atti Convegno di Studi Interazione Terremoto-Territorio in Provincia di Isernia, Isernia 14 Nov. 1992. GNDT-CNR, Archivio di Stato di Isernia, Osservatorio Vesuviano, 1-76.

Faccenna, C., Piromallo, C., Crespo-Blanc, A., Jolivet, L., Rossetti, F., 2004. Lateral slab deformation and the origin of the western Mediterranean arcs. Tectonics 23(1), TC1012 1-21. doi: 10.1029/2002TC001488.

Ferranti, L., 1997. Tettonica tardo Pliocenica-Quaternari dei Monti del Matese (Appennino Meridionale): raccorciamenti tardivi e distensione "neotettonica". Il Quaternario 10(2), 501–504.

Ferranti, L., Milano, G., Burrato, P., Palano, M., Cannavò, F., 2015. The seismogenic structure of the 2013–2014 Matese seismic sequence, Southern Italy: implication for the geometry of the Apennines active extensional belt., Geophys. J. Int. 201, 823–837.

Ferrarini, F., Boncio, P., Pappone, G., Cesarano, M., Aucelli, P.P.C., 2009. Nuovi dati su geometria, cinematica e segmentazione del sistema di faglie attive lungo il margine nord-orientale del Matese (Molise). Rend. Online Soc. Geol. It. 5, 100–103.

Fortini, P., 1805. Delle Cause de' Terremoti e Loro Effetti, Danni di Quelli Sofferti Dalla Città d'Isernia Fino a Quello de' 26 Luglio 1805. Sardelli, T., (ed.), Marinelli, Isernia, 1984, 65 pp.

Frezzotti, M., Giraudi, C., 1992. Evoluzione geologica tardo-pleistocenica ed olocenica del conoide complesso di Valle Majelama (Massiccio del Velino - Abruzzo). Il Quaternario 5, 33–50.

Galadini, F., Galli, P., 2000. Active tectonics in the central Apennines (Italy) – Input data for seismic hazard assessment. Natural Hazards 22, 202-223.

Galadini, F., Galli, P., 2004. The 346 A.D. earthquake (central-southern Italy): an archaeoseismological approach. Annals of Geophysics 47, 885-905.

Galli, P., Galadini, F., 2003. Disruptive earthquakes revealed by faulted archaeological relics in Samnium (Molise, southern Italy). Geophysical Research Letters 30, 1266. doi:10.1029/2002GL016456.

Galli, P., Scionti, V., 2006. Two unknown M>6 historical earthquakes revealed by palaeoseismological and archival researches in eastern Calabria (southern Italy): Seismotectonic implications. Terra Nova 18, 44–49, doi:10.1111/j.1365-3121.2005.00658.x.

Galli, P., Naso, G., 2009. Unmasking the 1349 earthquake source (southern Italy). Paleoseismological and archaeoseismological indications from the Aquae Iuliae fault. J. Structural Geology 31, 128-149.

Galli, P., Peronace, E., 2014. New paleoseismic data from the Irpinia fault. A different seismogenic perspective for southern Apennines (Italy). Earth Sci. Rev. 136, 175–201.

Galli, P., Peronace, E., 2015. Low slip rates and multimillennial return times for Mw 7 earthquake faults in southern Calabria (Italy). Geophys. Res. Lett., 42.

Galli, P., Galadini, F., Capini, S., 2002. Analisi archeosismologiche nel santuario di Ercole di Campochiaro (Matese). Evidenze di un terremoto distruttivo sconosciuto ed implicazioni sismotettoniche. Italian Journal of Quaternary Sciences 15(2), 151-163.

Galli, P., Giaccio, B., Messina, P., Naso, G., 2008a. L'influenza della tettonica attiva nello sviluppo di terrazzi alluvionali: il caso della faglia delle Aquae Iuliae nella media valle del Volturno (Venafro, appennino centro-meridionale). Extended abstracts of the 27° GNGTS Congress, Trieste 6-8 October 2008, 150-154.

Galli, P., Galadini, F., Pantosti D., 2008b. Twenty years of paleoseismology in Italy. Earth Science Review 88, 89-117. doi:10.1016/j.earscirev.2008.01.001.

Galli, P., Giaccio, B., Messina, P., Peronace, E., Zuppi, G.M., 2011. Palaeoseismology of the L'Aquila faults (central Italy, 2009, Mw 6.3 earthquake): implications for active fault linkage. Geophysical Journal International 187(3), 1119-1134.

Galli P., Messina P., Giaccio B., Peronace E., Quadrio B., 2012. Early Pleistocene to Late Holocene activity of the Magnola Fault (Fucino Fault System, central Italy), Bollettino di Geofisica Teorica ed Applicata, 53, 435-458.

Galli, P., Peronace, E., Quadrio, B., Esposito, G., 2014. Earthquake fingerprints along fault scarps: a case study of the Irpinia 1980 earthquake fault (southern Apennines). Geomorphology 206, 97–106.

Galli, P., Giaccio, B., Peronace, E., Messina, P., 2015. Holocene paleoearthquakes and early-late Pleistocene slip-rate on the Sulmona Fault (Central Apeninnes, Italy). Bull. Seismol. Soc. Am. 105(1), 1–13, doi:10.1785/0120140029.

Galli, P., Giaccio, B., Messina, P., Peronace, E., 2016. Three magnitude 7 earthquakes on a single fault in central Italy in 1400 years evidenced by new palaeoseismic results. Terra Nova, doi: 10.1111/ter.12202, in press.
Gemina, 1963. Ligniti e torbe dell'Italia continentale, ILTE, Torino, 319 pp.
Giaccio, B., Nomade, S., Wulf, S., Isaia, R., Sottili, G., Cavuoto, G., Galli, P., Messina, P., Sposato, A., Sulpizio, R., Zanchetta, G., 2012. The late MIS 5 Mediterranean tephra markers: a reappraisal from peninsular Italy terrestrial records. Quat. Sci. Rev. 56, 31–45.
Giaccio, B., Galli, P., Peronace, E., Arienzo, I., Nomade, S., Cavinato, G.P., Mancini, M., Messina, P., Sottili, G., 2014. A 560-440 ka tephra record from the Mercure basin, southern Italy: volcanological and tephrochronological implications. J. Quat. Sci. 29, 232-248.
Giannetti, B., 2001. Origin of the calderas and evolution of Roccamonfina volcano (Roman Region, Italy). J. Volcanol. 106(3-4), 301.
Giannetti, B., De Casa, G., 2000. Stratigraphy, chronology, and sedimentology of ignimbrites from the white trachytic tuff, Roccamonfina Volcano, Italy. Journal of Volcanology and Geothermal Research 96, 243-295.
Giraudi, C., Bodrato, G., Ricci Lucchi, M.,Cipriani, N., Villa, I.M., Giaccio, B., Zuppi, G.M., 2011. Middle and Late Pleistocene Glaciations in the Campo Felice basin (Central Apennines-Italy). Quaternary Research 75, 219–230.
Giuliani, R., D'Agostino, N., D'Anastasio, E., Mattone, M., Bonci, L., Calcaterra, S., Gambino, P., Merli, K., 2009. Active extension and strain accumulation in the Molise region (Southern Apennines, Central Italy). Boll. Geof. Teor. Appl. 50, 145-156.
Guerrieri, L., 2000. Evoluzione geologica recente della conca di Bojano e Sepino e possibili tendenze evolutive. Phd Thesis, Università degli Studi di Roma "La Sapienza", 171 pp.
Guerrieri L., Scarascia Mugnozza G., Vittori E., 1999. Analisi stratigrafica e geomorfologica della conoide tardo-quaternaria di Campochiaro ed implicazioni per la conca di Bojano in Molise, Il Quaternario, ltalian Journal of Quatemary Sciences, 12, 237-247.
Iorio, M., Liddicoat, J., Budillon, F., Incoronato, A., Coe, R.S., Insinga, D.D., Cassata, W.S., Lubritto, C., Angelino, A., Tamburrino, S., 2014. Combined palaeomagnetic secular variation and petrophysical records to time constrain geological and hazardous events: an example from the eastern Tyrrhenian Sea over the last 120 ka. Global and Planetary Changes 113, 91–109.
Lane, C.S., Brauer, A., Martín-Puertas, C., Blockley, S.P.E., Smith, V.C., Tomlinson, E.L., 2015. The Late Quaternary tephrostratigraphy of annually laminated sediments from Meerfelder Maar, Germany. Quaternary Science Reviews 122, 192–206
Le Bas, M.J., Le Maitre, R.W., Streckeisen, A., Zanettin, B., 1986. A chemical classification of volcanic rocks based on the total alkali–silica diagram. J. Petr. 27, 745–750.
Le Maitre, R.W., 2002. Igneous Rocks: A Classification and Glossary of Terms: Recommendations of the International Union of Geological Sciences, Subcommission on the Systematics of Igneous. Cambridge University Press, Rocks, 236 pp.
Loke M.H., 2001. Tutorial: 2-D and 3-D electrical imaging surveys, 127 pp., Geotomo Software, Malaysia.
Lotti, B., 1915. Contributo allo studio del terremoto del 13 gennaio 1915. Boll. Soc. Geol. It. 34, 283-296.
Lowe, D.J., 2011. Tephrochronology and its application: A review. Quaternary Geochronology 6, 107-153.
Machette, M.N., 1986. History of Quaternary offset and paleoseismicity along the La Jencia fault, central Rio Grande rift, New Mexico. Bull. Seismol. Soc. Am. 76, 259–272.
Machette, M.N., 1987. Preliminary assessment of paleoseismicity at White Sands Missile Range, southern New Mexico: evidence for recency of faulting, fault segmentation, and repeat intervals for major earthquakes in the region. Department of the Interior Geological Survey, Open-File Report, 87-444.

Magri, G., Molin, D., 1984. Il terremoto del dicembre 1456 nell'Appennino centro-meridionale. Comitato Nazionale Energia Nucleare, Rome, CNEN, 180 pp.
Malinverno, A., Ryan, W.B.F., 1986. Extension in the Tyrrhenian sea and shortening in the Apennines as result of arc migration driven by sinking of the lithosphere. Tectonics 5, 227–245.
Manetti, G., 1457. De Terraemotu Libri tres. In: Molin, D., Scopelliti, C., (Eds.). Collana commissione ENEA/ENEL per lo studio dei problemi sismici connessi con la realizzazione di impianti nucleari. Romana Editrice, Roma, 1983, 152 pp.
Mazzoli, S., Corrado, S., De Donatis, M., Scrocca, D., Butler, R.W.H., Di Bucci, D., Naso, G., Nicolai, C., Zucconi, V., 2000. Time and space variability of ‘‘thin-skinned’’ and ‘‘thick-skinned’’ thrust tectonics in the Apennines (Italy). Rend. Lincei, Sci. Fis. Nat. 9, 11(1), 5–39.
Meletti, C., Patacca, E., Scandone, P., Figliuolo B., 1988. Il terremoto del 1456 e la sua interpretazione nel quadro sismotettonico dell'Appennino meridionale. In: Figliuolo, B., Il terremoto del 1456. Edizioni Studi Storici Meridionali, Altavilla Silentina (SA), 1, 70-108; 2, 35-163.
Michetti A.M., Blumetti A.M., Esposito E., Ferreli L., Guerrieri L., Porfido S., Serva L., Vittori, E., 2000. Earthquake ground effects and seismic hazard assessment in Italy examples from the Matese and Irpinia areas, Southern Apennines, Active Fault Research for the New Millennium, Proceedings of the Hokudan Symposium and School on Active Faulting, 279-284.
Mostardini, F., Merlini, S., 1986. Appennino Centro Meridionale: sezioni geologiche e proposta di modello strutturale. Mem. Soc. Geol. Ital. 35, 177 – 202.
Nomade, S., Gauthier, A., Guillou, H., Pastre, J.F., 2010. 40Ar/39Ar temporal framework for the Alleret maar lacustrine sequence (French Massif-Central): Volcanological and paleoclimatic implications. Quaternary Geochronology 5, 20-27.
Pappalardo, L., Piochi, M., D’Antonio. M., Civetta, L., Petrini, R., 2002b. Evidence for multi-stage magmatic evolution during the past 60 ka at Campi Flegrei (Italy) deduced from Sr, Nd and Pb isotope data. J. Petrol. 43, 1415–1434.
Patacca, E., Sartori, R., Scandone, P., 1990. Tyrrhenian basin and Apenninic arcs: kinematic relations since Late Tortonian times. Memorie Società Geologica Italiana 45, 425–451.
Patacca, E., Scandone, P., 2007. Geological interpretation of the CROP-04 seismic line (southern Apennines, Italy). Boll. Soc. Geol. It. 7, 297–315.
Patacca, E., Scandone, P., Di Luzio, E., Cavinato, G.P., Parotto, M., 2008. Structural architecture of the central Apennines: Interpretation of the CROP 11 seismic profile from the Adriatic coast to the orographic divide. Tectonics 27, TC3006, doi:10.1029/2005TC001917.
Pepe, G., 1806. Ragguaglio istorico-fisico del tremuoto accaduto nel Regno di Napoli la sera de’ 26 luglio 1805. Napoli, 172 pp.
Peretto, C., Arnaud, J., Moggi-Cecchi, J., Manzi, G., Nomade, S., Pereira, A., Falguères, C., Bahain, J.J, Grimaud-Hervé, D., Berto, C., Sala, B., Lembo, G., Muttillo, B., Gallotti, R., Thun Hohenstein, U., Vaccaro, C., Coltorti, M., Arzarello, M., 2015. A human deciduous tooth and new 40Ar/39Ar dating results from the Middle Pleistocene archaeological site of Isernia la Pineta, southern Italy. PLoS ONE 10(10): e0140091. doi:10.1371/journal.pone.0140091.
Pierdominici, S., Heidbach, O., 2012. Stress field of Italy - Mean stress orientation at different depths and wave-length of the stress pattern. Tectonophysics 532-535, 301-311
Poli, G. S., 1806. Memoria sul Tremuoto de’ 26 Luglio del Corrente Anno. Napoli, presso Vincenzo Orsino. 224 pp.
Pondrelli, S., and Salimbeni, S., 2015. Regional Moment Tensor Review: An Example from the European–Mediterranean Region. Encyclopedia of Earthquake Engineering, DOI 10.1007/978-3-642-36197-5_301-1, 15 pp.
Porfido S., Esposito E., Vittori E., Tranfaglia G., Michetti A.M., Blumetti M., Ferreli L.,, Guerrieri L., and Serva L., 2002. Areal distribution of ground effects induced by strong earthquakes in the Southern Apennines (Italy), Surveys in Geophysics, 23, 529-562.

QRCMT, 2016. Quick Regional Moment Tensors. http://autorcmt.bo.ingv.it/quicks.html.

Rasmussen, S.O., Biglerb, M., Blockleyc, S.P., Bluniera, T., Buchardta, S.L., Clausena, H.B., Cvijanovica, I., Dahl-Jensena, D., Johnsena, S.J., Fischerb, H., Gkinisa, V., Guillevica, M., Hoekf, W.Z., Lowec, J.J., Pedroa, J.B., Poppa, T., Seierstada, I.K., Steffensena, J.P., Svenssona, A.M., Vallelongaa, P., Vinthera, B.M., Walkerh, M.J.C., Wheatleyj, J.J., Winstrupa, M., 2014. A stratigraphic framework for abrupt climatic changes during the last glacial period based on three synchronized Greenland ice-core records: Refining and extending the INTIMATE event stratigraphy. Quat. Sci. Rev. 106, 14–28, doi:10.1016/j.quascirev.2014.09.007.

Regattieri, E., Giaccio, B., Zanchetta, G., Drysdale, R.N., Galli, P., Nomade, S., Peronace, E., Wulf, S., 2015. Hydrological variability over the Apennines during the Early Last Glacial precession minimum, as revealed by a stable isotope record from Sulmona basin, Central Italy. J. Quat. Sci. 30(1), 19-31.

Reilinger, R., McClusky, S., Vernant, P., Lawrence, S., Ergintav, S., Cakmak, R., Ozener, H., Kadirov, F., Guliev, I., Stepanyan, R., Nadariya, M., Galaktion, H., Mahmoud, S., Sakr, K., ArRajehi, A., Paradissis, D., Al-Aydrus, A., Prilepin, M., Guseva, T., Evren, E., Dmitrotsa, A., Filikov, S.V., Gomez, F., Al-Ghazzi, R., Karam, G., 2006. GPS constraints on continental deformation in the Africa-Arabia-Eurasia continental collision zone and implications for the dynamics of plate interactions. J. Geophys. Res., BO5411, doi:10.1029/2005JB004051.

Roberts G.P., Michetti A.M., 2004. Spatial and temporal variations in growth rates along active normal fault systems: an example from the Lazio-Abruzzo Apennines, central Italy. J. Struct. Geol., 26, 339-376.

Romano, V., 2010. Prospezione ed analisi gravimetrica della conca di Bojano (Molise), Bachelor's Degree, "La Sapienza" University, Rome, 37 pp.

Rouchon, V., Gillot, P.Y., Quidelleur, X., Chiesa, S., Floris, B., 2008. Temporal evolution of the Roccamonfina volcanic complex (Pleistocene), Central Italy. Journal of Volcanology and Geothermal Research 177(2), 500-514.

Royden, L., Patacca, E., Scandone, P., 1987. Segmentation and configuration of subducted lithosphere in Italy: an important control on thrust-belt and foredeep-basin evolution. Geology 15, 714–717.

Russo, F., Terribile, F., 1995. Osservazioni geomorfologiche, stratigrafiche e pedologiche sul Quaternario del Bacino di Bojano (Campobasso). Il Quaternario 8, 239-254.

Sieberg, A., 1930. Geologie der Erdbeben. Handboch der Geophysic 2(4), 552-554. Berlin.

Stuiver, M., Reimer, P.J., Reimer, R., 2010. CALIB Radiocarbon Calibration, execute version 7.1. web site: http://calib.qub.ac.uk/calib/.

Tomlinson, E.L., Arienzo, I., Civetta, L., Wulf, S., Smith, V.C., Hardiman, M., Lane, C.S., Carandente, A., Orsi, G., Rosi, M., Müller, W., Thirlwall, M.F., Menzies, M.A., 2012. Geochemistry of the Phlegrean Fields (Italy) proximal sources for major Mediterranean tephras. Geochim. Cosmochim. Acta 93, 102–128.

Wallace, R.E., 1977. Profiles and ages of young fault scarps, north-central Nevada. Geol. Soc. Am. Bull. 88, 1267–1281.

Wallace, R.E., 1984. Fault scarps formed during the earthquakes of October 2, 1915. Pleasant Valley, Nevada, and some tectonic implications. U.S. Geol. Survey Prof. Paper, 1274-A, 32 pp.

Wells, D.L., Coppersmith, K.J., 1994. New empirical relationships among magnitude, rupture length, rupture width, rupture area, and surface displacement. Bull. Seism. Soc. Am. 84, 974–1002.

Working Group CPTI, 2011. CPTI11, the 2011 version of the Parametric Catalogue of Italian Earthquakes. Rovida, A., Camassi, R., Gasperini, P., Stucchi, M., (eds). Istituto Nazionale di Geofisica e Vulcanologia, Milano, Bologna. DOI: http://doi.org/10.6092/INGV.IT-CPTI11.

Wulf, S., Keller, J., Paterne, M., Mingram, J., Lauterbach, S., Opitz, S., Sottili, G., Giaccio, B., Albert, P., Satow, C., Viccaro, M., Brauer, A., 2012. The 100-133 record of Italian explosive volcanism and revised tephrochronology of Lago Grande di Monticchio. Quaternary Science Reviews 58, 104-123.

1296